Check for updates

Non-equilibrium plasma co-upcycling of waste plastics and CO_2 for carbon-negative oleochemicals†

Harish Radhakrishnan, [ID] ‡[a] Samirah Gnangbe,‡[a] Alif Duereh,[a] Sultan Ul Iffat Uday,[a] Lusi A, [ID][a] Haiyang Hu,[b] Hui Hu,[b] Mark Mba Wright [ID] *[a] and Xianglan Bai [ID] *[a,c]

Mechanical recycling and chemical upcycling by thermochemical reactions have been the major approaches for recycling end-of-life plastics. Herein, we report an electrified approach to upcycle waste plastics into carbon-negative commodity chemicals using greenhouse gas CO_2 as the oxidant and additional carbon source. In this non-equilibrium plasma process, waste polyolefins were oxidatively depolymerized by plasma-activated CO_2 to produce oleochemicals and hydrocarbon chemicals in a single-step process at high reaction rates. In addition, a mixture of CO_2 and a small amount of O_2 was employed as plasma gases to selectively produce fatty alcohols from polyolefins. Based on this atmospheric pressure, non-solvent, and non-catalyst process, up to 97.6% of fatty alcohols could be produced within minutes. In this article, the co-conversion approach was demonstrated using common polyolefins and real-world mixed waste plastics to obtain comparable results. The techno-economic analysis estimates the internal rate of return to be 42.2% and 43.5% for the plasma-based conversion of waste plastics, depending on the plasma gas composition. Lifecycle assessment indicates the global warming potential is between −3.33 and −3.07 kg CO_{2e} per kg of plastic.

1. Introduction

The utilization of plastic materials has grown over the years because of their lightweight, low-cost, durability, and processability attributes.[1,2] Plastics can be shaped into various products for several applications, such as packaging, automotive, electronics, and medical applications. An alarming consequence of the rise in production and usage is the amount of plastic waste generated and its inefficient management leading to plastic pollution.

Global plastic production reached 390.7 million metric tons (MMT) in 2021, which corresponds to a significant increase of 44% within ten years.[3] Single-use plastics, mainly composed of polyolefins, constitute over 50% of the plastic production.[4] United States (US) generated the largest quantity of plastics, accounting for 18% of global production, after China.[3] The EPA reported that 4.5 MMT out of 32.4 MMT of plastic gener-

ated in the US in 2018 were recycled, ~15% were incinerated, and the remaining waste was disposed of into landfills.[5] Polyolefins, such as polyethylene (PE) and polypropylene (PP), have a meager recycling rate and are discarded in landfills or oceans.[4] Waste plastic litter is piling up in rivers, oceans, and soil, posing adverse effects on the environment and human health.[4]

Recycling, incineration, and landfilling are the most common methods to manage waste plastics. However, they are found to be ineffective in managing plastic waste. Landfilling occupies valuable land, emits greenhouse gases, including CH_4 and CO_2, and pollutes the aquifer.[6] The conversion of waste to energy through incineration releases CO_2 and toxic chemicals into the atmosphere. Additionally, mechanical recycling has several limitations, including challenges in handling contaminated and mixed waste streams and the decrease in the mechanical properties of the materials at each cycle, resulting in downcycling.[6]

Research efforts have been undertaken to explore technologies to increase the value of plastic waste. Plastics are made from fossil fuels and contain hydrocarbon resources that can be recovered and converted to valuable chemicals at their end-of-life. Thermochemical conversion has been considered a promising technology to upcycle plastic waste and reduce waste disposal in landfills and natural habitats.[1] Pyrolysis and gasification are the most industrialized chemical recycling

[a]Department of Mechanical Engineering, Iowa State University, Ames, IA, 50011, USA. E-mail: bxl9801@iastate.edu
[b]Department of Aerospace Engineering, Iowa State University, Ames, IA, 50011, USA
[c]Department of Chemical & Biological Engineering, Iowa State University, Ames, IA, 50011, USA
†Electronic supplementary information (ESI) available. See DOI: https://doi.org/10.1039/d4gc02340d
‡Co-first authors.

technologies.[1,6] However, these endothermic reactions require high energy input to depolymerize and decompose plastics.[6] Plastic waste gasification occurs at 750–900 °C in the presence of steam or oxygen to yield a gaseous product known as syngas. The latter requires intensive cleaning to remove tar and contaminants and additional upgrading processes to produce marketable commodities.[7] Pyrolysis of polyolefins is performed under oxygen-starved conditions at 500–700 °C (or lower than 500 °C when pressures and extended conversion times are allowed) to produce wax and oil, a complex long-chain hydrocarbon mixture.[8] Pyrolysis products can be regarded as low-value, which requires further upgrading, such as thermal catalytic or hydroformylation, to generate transportation fuel or chemical commodities.[1]

Other sustainable techniques, which can convert polyolefins into value-added products at low energy requirements, have gained greater interest. Recent studies identified non-equilibrium plasma processes as a viable technology for producing light hydrocarbons and hydrogen from plastic waste at low temperatures and atmospheric pressure operations.[9] Plasma, often referred to as the "fourth state of matter," is an ionized gas composed of free electrons and heavy species such as atoms, ions, and molecules.[10] Plasma is created by applying electrical discharge to a gas and is generally classified as either thermal or non-thermal, depending on the energy level. Thermal plasma operates at high temperature, 6000–20 000 K, and the electrons and heavy particles are in thermal equilibrium.[11] On the contrary, non-thermal plasma (NTP) performs at non-equilibrium conditions, where the gas temperature can remain as low as room temperature while the electron temperature can range from 10 000–100 000 K.[10]

The energy levels of plasma species are high and can break any hydrocarbon chains without an external heating source. Thermal plasma is a well-established technology in metallurgical processing, hazardous waste treatment, and solid waste treatment.[12] In recent decades, thermal plasma for waste plastic treatment has been intensively examined, leading to the construction of pilot plants.[11,13] The high energy density and high temperature of thermal plasma result in low thermal efficiency and product selectivity, and it is also associated with high capital and operational costs when executed on a large scale.[11,14] On the other hand, non-thermal plasma processes offer greater energy efficiency and selectivity in plasma chemical reactions. Under non-thermal plasma discharge, the collision between high-temperature electrons and cold gas molecules leads to the generation of radicals, ions, activated atoms and molecules. Energetic electrons and active particles generated by plasma discharge can break a wide range of chemical bonds without needing to establish thermodynamic equilibrium. Since the reactions occur under non-equilibrium conditions, thermodynamically unfavorable reactions can proceed with plasma at unconventionally low temperatures.[10,15–17] This distinctive property makes this process chemically selective and advantageous for synthesizing fuels and chemicals from plastic waste. Several experimental studies have reported using non-thermal plasma to decompose PE into hydrogen and light

hydrocarbons.[9,11,18–20] For instance, Yao *et al.*[19] used non-thermal plasma-activated H_2 to deconstruct high-density PE to lower alkanes (C_1–C_3). Diaz-Silvarrey *et al.*[21] applied nitrogen plasma to crack PE pyrolysis vapor containing long-chain hydrocarbons into ethylene-rich gases. Rather than plastics, previous studies also applied non-thermal plasma to CO_2 and single molecules (H_2, H_2O, or CH_4) to produce synthetic fuel or other higher-value platform chemicals.[10,22] While non-thermal plasma has been recognized as an efficient pathway to upcycle biomass and various waste streams to in-demand products with excellent potential for scale-up,[9,10] the technical and economic feasibility of non-thermal plasma for plastic waste conversion has not yet been verified.

In this article, we present a novel process to co-upcycle plastic wastes and waste CO_2 to commodity chemicals using a non-equilibrium plasma approach developed and demonstrated at a laboratory scale. Based on the experimental results in this work, we evaluated the technical feasibility and economic viability of producing oleochemicals from waste resources. Additionally, we performed a life cycle assessment (LCA) to investigate the global warming potential (GWP) of this technology.

Oleochemicals, such as fatty alcohols and fatty acids, are employed in various industries, such as cosmetics, pharmaceuticals, lubricants, plastic, and surfactants. The global market was valued at $22.66 billion in 2022 and is forecasted to grow at a compound annual growth rate (CAGR) of 7.1% from 2023 to 2030.[23] Oleochemicals not only have a substantial market size but also are valuable chemical commodities. These chemicals have many industrial applications. Fatty alcohol mixtures find direct applications such as emollients, emulsifiers, and thickeners in cosmetics.[24] Long-chain fatty alcohols as a mixture form ($C_{12}+$) are widely used as intermediates in the production of surfactants and detergents, while C_5–C_{12} fatty alcohols find applications as plasticizers in polymer production and solvents in coatings and resin formulations.[24–26] Fatty acids can be used as cosmetic and food additives and have wide applications in textile treatment and in producing surfactants, soaps, and detergents.[24,25] Further, fatty acids are also used as intermediates in the production of esters, amines, and amides.[25] In 2022, the market prices of fatty alcohol and fatty acid were $2.5–3 per kg and $1.6–1.9 per kg, respectively,[27,28] much higher than hydrocarbons of the same chain length. The cost of oleochemicals can be associated with the feedstock used and the production process. Conventionally, fatty alcohol is manufactured from petrochemicals or palm kernel oil. Fossil-derived fatty alcohol is produced *via* the Ziegler or oxo process, which involves multi-step processes such as the alkylation of ethylene using a hydrogenated catalyst and hydroformylation of long-chain olefins utilizing syngas.[29] Such methods are energy-intensive, and the life cycle greenhouse gas (GHG) emission for 1 kg of fatty alcohol is estimated to be 2.97 kg CO_{2e}.[29,30] Meanwhile, palm kernel oil-derived fatty alcohol was found to have a high GHG emission of 5.27 kg CO_{2e} due to the land use change for palm oil plantations.[29] Hence, producing oleochemicals from

less energy-intensive pathways and abundant feedstock, like plastic waste, would be beneficial in minimizing GHG emissions. In their recent study, Li *et al.*[31] produced fatty alcohols from polyolefin waste through a multi-step process involving pyrolysis, hydroformylation, and hydrogenation. The GHG of converting 1 kg of plastic waste using this process was calculated at 1.6 kg CO_{2e}, lower than the conventionally produced fatty alcohols.
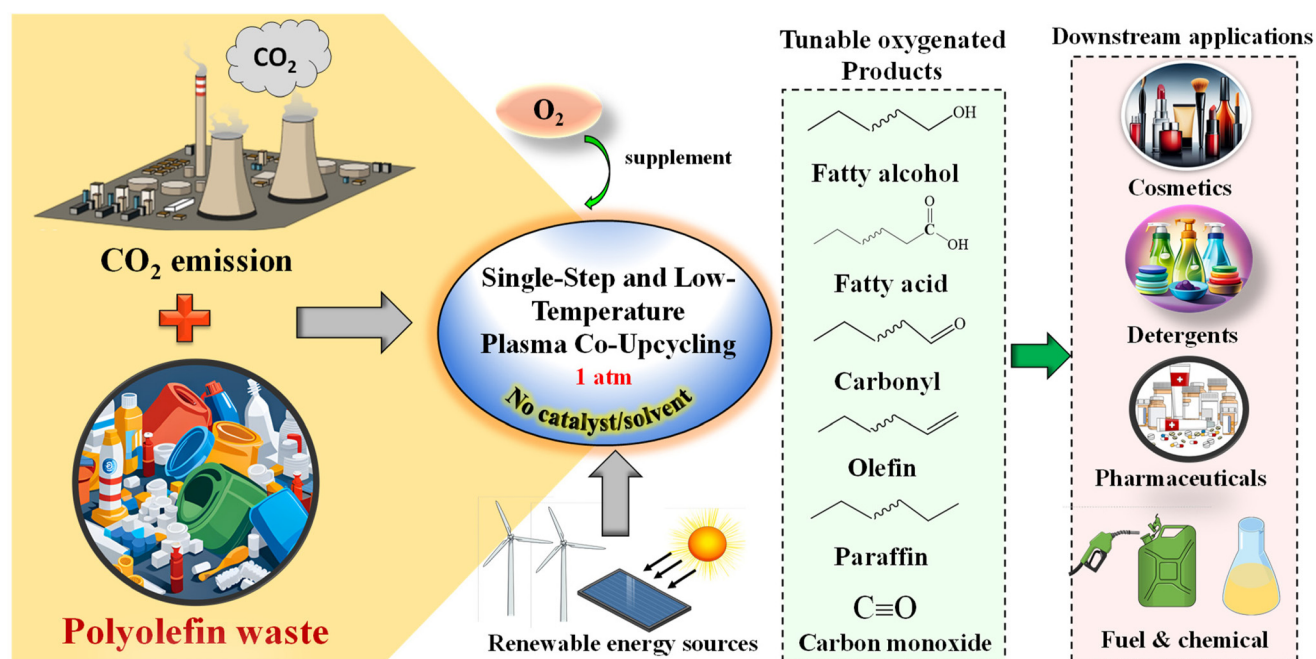
In our recent study, a single-step process was developed to produce oleochemicals and hydrocarbons from waste plastics and plasma-activated CO_2. The reaction system was also tailored to selectively produce fatty alcohols by introducing a small amount of O_2. An isotopic study was performed to confirm the role of polyolefin as a sink for chemically capturing CO_2. The applicability of the selective co-conversion by plasma was also demonstrated using common polyolefins and real-world mixed polyolefins. Technoeconomic analysis (TEA) and LCA results suggest this non-thermal plasma, catalyst and solvent-free approach can produce carbon-negative chemicals and fuels using wastes at low costs. The concept of green upcycling of waste plastics and CO_2 for carbon-negative commodity chemicals is illustrated in Scheme 1.

2. Results and discussion

2.1. PE conversion using CO_2 plasma

Product distribution per PE. We converted high-density PE using a co-axial dielectric discharge barrier (DBD) plasma reactor operating under a continuous-flow semi-batch configuration and atmospheric pressure (Fig. S1†). Plastics were converted inside the horizontally placed reactor powered by an alternative current (AC) electric source. The reaction gas entered one end of the reactor and the vapor products exiting at the other were collected in condensers. Non-condensable gases were analyzed online. Before the plasma actuation, the reactor was externally heated for 3–4 min to melt plastics so that the plastic particles do not fall off from the reaction zone. External heating was terminated once the reactor reached a target temperature between 300 and 400 °C so that plasma energy became the sole power source. The plasma conversion was carried out by varying plasma power source voltage (V), frequency (f), gas residence time (t_R), and the initial reactor temperature (T_i) after the preheating. The gas residence time was controlled by changing the gas flow rate at the reactor inlet. The reaction conditions of PE and other types of plastics are provided in Table 1 and apply to the rest of this article. Plasma power input and average inner reactor gas temperatures for PE conversion are given in Table S1.† The reproducibility of the experiments from typical tests is given in Table S2.† The time-dependent product distributions calculated per PE mass are reported in Fig. 1. Under the reaction condition of (f of 8 kHz, t_R of 13 s, and T_i of 350 °C), the voltage of 12.5 kV (case A) was the threshold for initiating plasma discharge. In the absence of external heating, the reactor temperature decreased with an increasing plasma discharge time. Due to low power (44 W) and average reactor temperature (252 °C during a 10 min plasma discharge), PE conversion at this reaction condition was minimal (products were not analyzed). Employing higher voltages of 15 kV (case B) and 17.5 kV (case C) caused increases in the plasma power (98 W at case B or 138 W at case C) and the reactor tempera-

Scheme 1 Concept of plasma co-upcycling waste plastics and CO_2. CO_2 serves as an oxidant and carbon source to depolymerize polyolefins into platform chemicals, whereas plastics enhance CO_2 conversion. Fatty alcohols are selectively produced by adding O_2.
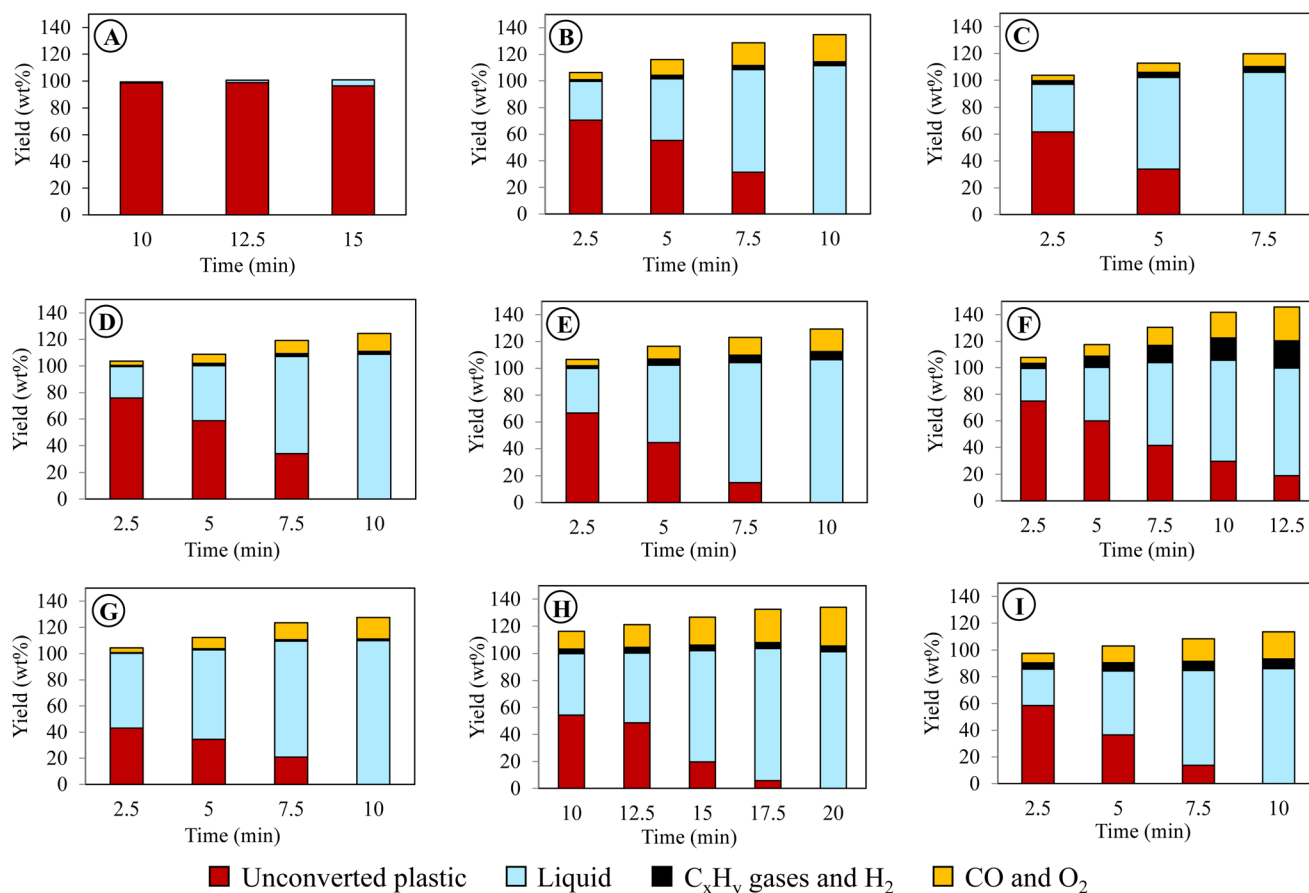
Table 1 Nomenclatures for tests performed with different plastics and reaction conditions, apply to the rest of the article.

Condition	Feed	Gas	T_i (°C)	t_R (s)	V (kV)	f (kHz)	Time (min)
A	PE	CO_2	350	13	12.5	8	15
B	PE	CO_2	350	13	15	8	10
C	PE	CO_2	350	13	17.5	8	7.5
D	PE	CO_2	350	13	15	7.5	10
E	PE	CO_2	350	13	15	8.5	10
F	PE	CO_2	350	10	15	8	12.5
G	PE	CO_2	350	20	15	8	10
H	PE	CO_2	300	13	15	8	20
I	PE	CO_2	400	13	15	8	10
J	PE	$CO_2/8\% O_2$	350	13	15	8	10
K	PE	$CO_2/8\% O_2$	350	20	15	8	7.5
L	PE	$CO_2/14\% O_2$	350	13	15	8	7.5
M	LDPE	CO_2	325	20	15	8	10
N	PP	CO_2	325	20	15	8	10
O	LDPE	$CO_2/8\% O_2$	350	13	15	8	10
P	PP	$CO_2/8\% O_2$	350	13	15	8	10
Q	PC-PE	CO_2	325	20	15	8	10
R	PC-PE	$CO_2/8\% O_2$	350	13	15	8	10

In the above, T_i is the initial temperature before plasma discharge, CO_2/O_2 concentration is represented in vol%, t_R is the vapor-phase gas residence time, V is the voltage, f is the frequency, and "Time" is the reaction completion time. This nomenclature applies for the entire article including ESI.†

ture (339 °C at case B or 396 °C at case C). The higher temperatures with higher voltages are due to an increased Joule heating effect caused by stronger plasma intensity. Increasing voltage strongly enhanced the PE conversion rate. With case B, PE completely devolatilized within 10 min to produce 111.4% liquid and 23.4% gases (both per PE mass). The liquid product mass exceeded PE feedstock mass, indicating CO_2 was also converted to the liquid products. The complete conversion of PE was achieved within 7.5 min in case C with the higher voltage, producing 105.9% liquid and 13.8% gases. Since 15 kV was the optimal voltage for obtaining a higher liquid yield, this voltage was used in the rest of the tests. It was found that increasing electricity frequency also increases the plasma power and the reactor temperature. Among the three frequencies of 7.5 kHz (case D), 8 kHz (case B), and 8.5 kHz (case E), 8 kHz (case B) was the optimal frequency for producing the highest liquid yield (111.4%). Although PE conversion was slightly faster with case E, the liquid yield became lower (106.4%). Thus, 15 kV and 8 kHz were used to evaluate the effect of the gas resistance times. Reducing the gas residence time, t_R, from 13 s (case B) to 10 s (case F) decreased plasma power (98 W to 89 W) and lowered the reactor temperature (339 °C to 299 °C). The shorter t_R also significantly lowered PE

Fig. 1 Time-dependent product distribution calculated per initial PE mass for different plasma conditions. Refer to Table 1 for the alphabetical nomenclatures in circles and their corresponding reaction conditions.

conversion, resulting in 80.6% liquid and 19% unconverted PE after 12.5 min. The gas yield at this condition was 45.9% due to the higher flow rate and the higher total amount of CO_2 entering the reactor. On the other hand, increasing t_R from 13 s to 20 s (case G) led to increased plasma power (100 W), higher reactor temperature (353 °C), and higher PE conversion rate. After a 10 min conversion at case G, the liquid and gas yields were 109.9% and 17.7% compared to 111.4% and 23.4% obtained at case B with t_R of 13 s. Three different initial reactor temperatures, T_i, at plasma actuation were also compared, which are 300 °C (case H), 350 °C (case B), and 400 °C (case I). Although reactor preheating is not required to generate plasma or convert plastics, the plasma reactor with a higher T_i can reduce the dielectric breakdown voltage for initiating plasma discharge and increase plasma intensity. It was found that increasing T_i increased plasma power (90, 98, and 111 W with cases H, B, and I) and the average reactor temperature (266, 339, and 395 °C). PE conversion rate and product distribution were strongly affected by T_i. While 111.4% liquid and 23.4% gases were produced within 10 min at case B with T_i of 350 °C, it took 20 min to produce 101.2% liquid and 32.8% gases at case H with T_i of 300 °C. Although the PE conversion rate was the highest at case I with T_i of 400 °C, the liquid yield after 10 min was only 86.1% (gas yield of 27.4%), significantly lower than those produced using lower T_is. Plasma characterizations for different test conditions are included in Fig. S2.†

Thermal effect during PE conversion. The average reactor temperatures during the PE conversion by CO_2 plasma ranged from 266 to 395 °C, depending on the reaction conditions. To distinguish thermal decomposition and plasma conversion, PE and CO_2 in the reactor were externally heated without applying plasma. There was no mass loss of PE after the 3–4 min reactor preheating before the plasma initiation. The gas chromatography-mass spectrometry (GC/MS) analysis of the molten plastic did not detect compounds (Fig. S3(a)†), confirming no noticeable PE degradation during the reactor preheating stage. Furthermore, thermally heating the reactor for 20 min at 350 °C or 400 °C only caused 5% or 12% PE mass loss. The GC/MS analysis of the minor waxy products recovered from the condensers after the heating showed alkanes and alkanes with distributed carbon numbers (Fig. S3(b)†). These results align with previous knowledge that PE is thermally stable below 400 °C. The onset temperature for thermal decomposition and vapor volatilization is about 430 °C for PE.[32–35] Pyrolysis of PE under atmospheric pressure had to be performed at temperatures of 500 °C and above to volatilize hydrocarbon wax and oil products.[1,32–35] Although PE was previously converted at lower temperatures (350–450 °C), the conversion takes up to hours and requires pressurized reactors and catalysts.[1] The reactor temperatures in this work were also too low to dissociate CO_2 thermally.[35] Accordingly, the results confirm that the reactor temperature, pressure, and reaction time of our system were insufficient to activate CO_2 or meaningfully convert PE without plasma discharge. Because thermodynamically equilibrium conditions are not required for non-

thermal plasma discharge, PE depolymerization and CO_2 conversion can occur at unconventionally low temperatures.

PE conversion by argon and air plasma. The effectiveness of CO_2 plasma for converting PE was also compared by replacing CO_2 with argon or air gas in the same plasma reactor and condition of case B. Complete conversion of PE took 45 min with argon plasma or 15 min with air plasma, producing 69.0% or 112.9% of liquids (Fig. S4 and S5† for time-resolved product yields and liquid composition). Therefore, plasma-activated CO_2 was more effective and had higher reaction rates than air or argon plasma in depolymerizing PE.

Gas composition from PE conversion by CO_2 plasma. Gas products from the CO_2 plasma conversion of PE comprised CO, O_2, H_2, and light hydrocarbons (C_1–C_5 alkanes and alkenes). Their product yields calculated per PE mass can be found in Fig. 1 along with liquids and solid yields. The sum yield of H_2 and hydrocarbon gases only accounted for 3% of PE with case B (V = 15 kV, f = 8 kHz, t_R = 13 s, T_i = 350 °C), indicating that PE carbon and hydrogen mainly converted to liquid products rather than fuel gases. Increasing voltage (case C) or frequency (case E) increased H_2 and hydrocarbon gases, which were also accompanied by decreased liquid yields. On the other hand, the sum yield of H_2 and hydrocarbon gases decreased to 1.3% with a longer t_R of 20 s (case G) and increased to 20.6% with a shorter t_R to 10 s (case F). Longer residence time corresponds to increased interactions between CO_2 and PE under plasma discharge, promoting the reaction rate and the conversion of PE to condensable molecules rather than gases. For different initial temperatures, case B (350 °C) resulted in the lowest sum yield of H_2 and hydrocarbon gases (3%). The yield increased to 7.3% at case H (400 °C) and 4.4% at case I (300 °C), suggesting more PE turns into gaseous products at higher or lower temperatures.

The gas selectivity for different reaction conditions is provided in Fig. 2. CO was the primary gas product in all conditions, with its selectivity ranging from 50% to 90.3%. The highest and lowest CO selectivity was observed with the longest gas residence time (case G) and the highest initial temperature (case I), respectively. Although dissociation of 1 mol of CO_2 theoretically produces 1 mol of CO and 0.5 mol of O_2, O_2 content in the gas stream was nearly negligible. Thus, CO_2-derived O was preferentially used to oxidize the liquid molecules.

Liquid characterization for PE conversion by CO_2 plasma. The chemical compositions of the liquids were analyzed using high-temperature GC/MS (HT-GC/MS). The elemental C, H, and O contents in the liquids were measured by an elemental analyzer. The liquids consisted of oxygenated compounds (fatty alcohols, fatty acids, and carbonyls) and hydrocarbons (olefins and paraffins) with distributed carbon chain lengths. The product yields based on their carbon number ranges and elemental compositions of the whole liquids are given in Table 2 and the product functional group yields and oxygen content of the corresponding liquids are plotted in Fig. 3. The liquid compositions were also validated by conducting ^{13}C NMR analysis (Fig. 4(a(i))). The NMR spectrum exhibits the
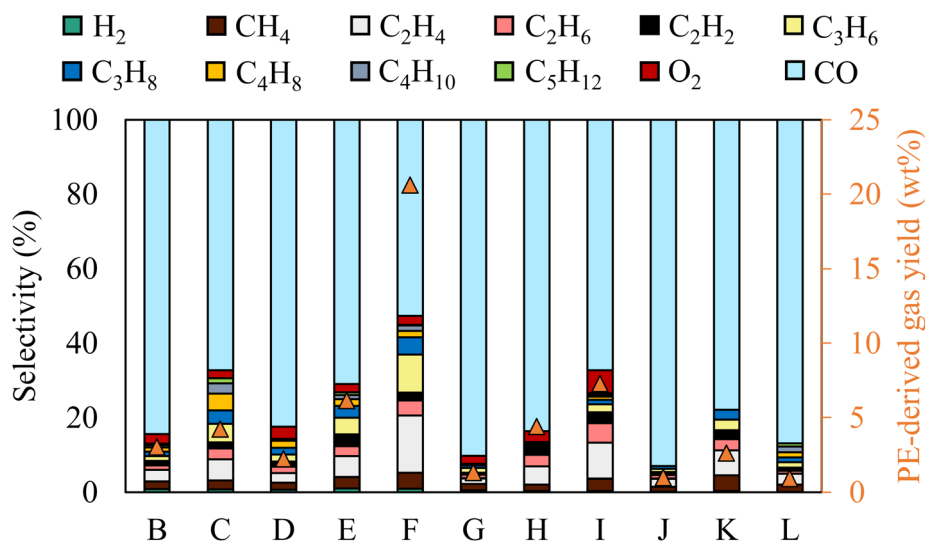
Fig. 2 Gas product selectivity and PE-derived gas yield (H_2 and C_xH_y) for different reaction conditions.

Table 2 Characterization of liquids obtained using different reaction conditions

Condition	Liquid yield (wt%)	Product carbon number distribution (wt%)				Elemental analysis (wt%)		
		C_5–C_{12}	C_{13}–C_{20}	C_{21}–C_{28}	C_{28}^+	C (%)	H (%)	O (%)
B	111.4	28.2	23.4	22.6	37.2	80.9	12.9	6.2
C	105.9	39.6	33.3	20.1	12.9	82.2	13.1	4.7
D	108.8	22.4	21.9	21.2	43.3	81.2	13	5.8
E	106.4	39.1	25.2	27.1	15.0	80.6	13.1	6.3
F	80.6	15.6	13.1	12.0	39.9	82.8	13.3	3.9
G	109.9	50.1	24.4	19.2	16.2	79.6	12.6	7.8
H	101.2	29.8	24.2	10.5	36.7	81.5	13.1	5.4
I	86.1	18.5	16.8	43.3	7.5	84.9	13.5	1.7
J	120.7	64.4	37.1	13.2	6.0	76.7	12.1	11.2
K	115.3	61.0	41.2	12.9	0.0	78.1	12.1	9.8
L	110.8	56.7	29.2	16.5	8.4	76.8	12.2	11.0
M	105.8	31.5	53.8	15.2	5.2	78.8	12.5	7.5
N	98.1	36.5	40.8	17.0	3.8	78.7	12.5	7.6
O	113.5	76.7	22.5	6.5	7.8	76.8	12.2	11.0
P	109.5	66.8	30.5	7.6	4.7	77.2	12.3	10.5
Q	104.4	61.1	23.3	11.1	8.9	80.5	12.4	7.1
R	111.1	60.1	32.7	15.6	2.6	77.0	12.1	10.9

Products from case A were not analyzed due to low conversion.

peaks of alcohols (OH, δ = 60–95 ppm), carboxylic acids (COOH, δ = 175–180 ppm), carbonyls (C=O, δ = 180–210 ppm), R–CH=CH$_2$ bonds (δ = 135–140 ppm), methyl (–CH$_3$, δ = 10–20 ppm) and methylene (–CH$_2$, δ = 110–15 ppm), supporting the GC/MS analysis results. As shown in Table 2, the cases with higher voltage, higher frequency, longer gas resistance time, and higher initial temperature resulted in liquids with narrower molecular weight distributions of shorter-carbon chain-length compounds, attributing to the higher degrees of PE depolymerization and β–β carbon scissions. However, the oxygen content of the liquids did not follow the exact trend as their carbon chain-length distributions. Liquid oxygen content was 6.2% in case B, with the highest liquid yield. However, increasing the voltage caused a decrease in oxygen content to 4.7% in case C. In comparison, increasing frequency at case E

had no significant impact on the oxygen content. The liquid with the highest oxygen content of 7.8% was obtained in case G with t_R of 20 s, compared to 6.2% in case B with t_R of 13 s and 3.9% in case F with t_R of 10 s. Thus, the longer gas residence time was beneficial in enhancing oxidative depolymerization of PE. The initial temperature also had a significant impact on PE oxidation. While the liquid oxygen content was 6.2% in case B with T_i of 350 °C and 5.3% in case H with 300 °C, it was only 1.7% in case I with 400 °C despite this case having a higher average reactor temperature during plasma discharge than the other two cases.

Notably, the oxygen content in liquids was not contributed by water as the amounts of water produced in this work were negligible (<0.7%, Table S3†). The oxygen content of the liquids well corresponded to the abundance of oleochemicals
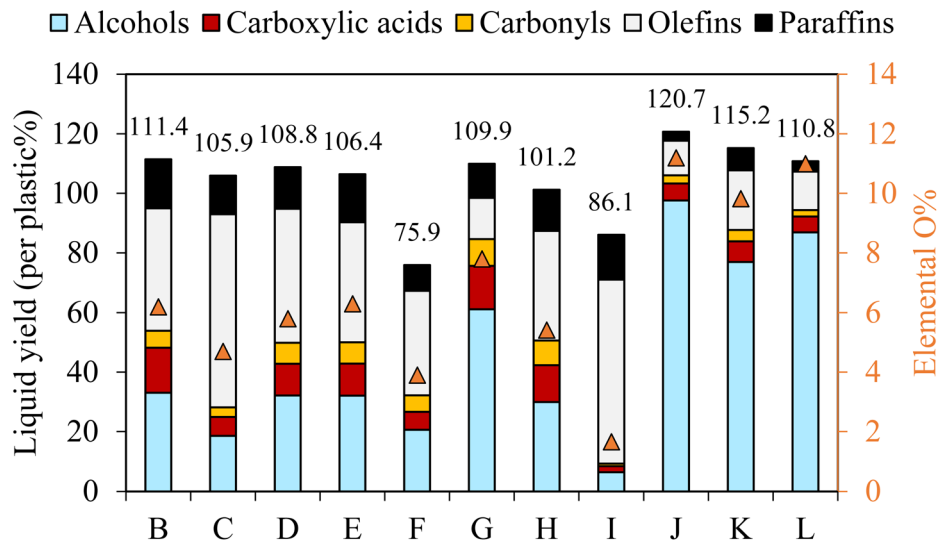
Fig. 3 Liquid product compositions and oxygen content for PE conversion using different reaction conditions.

products. Case B resulted in 33% fatty alcohols, 15.2% fatty acids, and 5.7% carbonyls, totaling 53.9% (or 48.4% per liquid) oxygenated compounds. The rest included 41.1% of olefins and 16.5% of paraffins. Increasing voltage in case C reduced the oxygenated products, whereas it increased the hydrocarbons. The frequency effect was less noticeable in case E than the voltage effect. The highest yield of total oxygenated products was obtained in case G with the longest gas residence time, producing 61.1% of fatty alcohols, 14.5% of fatty acids, and 9.0% of carbonyls with a total 84.6% of oxygenated products (or 77.0% per liquid) (Fig. 3). The rest included 13.1% olefins and 11.4% paraffin. As described earlier, the sum yield of H_2 and hydrocarbon gases was the lowest in this case because more PE elements are converted to oleochemicals. As predicted from its oxygen content, the liquid produced at case I with the highest initial temperature of 400 °C was mainly hydrocarbons (61.7% olefins and 15% paraffin). The total oxygenated compounds were only 9.3% in this case. In comparison, case H, with the lowest initial temperature of 300 °C, could still produce 50.6% oxygenated compounds, although it took longer to convert PE.

As shown above, the plasma-activated CO_2 can effectively depolymerize and oxidize PE to produce oleochemicals, olefins, and paraffin in high product yields. Among the variables, gas residence time and initial reactor temperature had the most pronounced effects on oleochemical selectivity. Case G, with the longest gas residence time, delivered the liquid with the highest oleochemical yields and narrower molecular distribution. As described earlier, the gaseous product with the highest CO selectivity was also observed in this case.

2.2. PE conversion by CO_2/O_2 plasma

The chemical selectivity of PE conversion by CO_2 plasma was further tailored by entraining small amounts of O_2 to CO_2 at the reactor inlet. Three CO_2/O_2 plasma conditions were studied by varying gas residence time and O_2 concentration (cases J, K and L). The plasma power and the reactor gas temperature for the respective cases are included in Table S1† to compare with the CO_2 plasma-base conversion. Employing CO_2/O_2 plasma reduced plasma power compared to using CO_2 plasma, from 98 W in case B (0% O_2 and 13 s) to 84 W in case J (8 vol% O_2 and 13 s), and 75 W in case K (14 vol% O_2 and 13 s), and from 100 W in case G (0% O_2 and 20 s) to 77 W in case L (8 vol% O_2 and 20 s). On the other hand, it increased the average reactor gas temperature from 339 °C to 344 °C and 370 °C, and from 353 °C to 367 °C in the corresponding cases. The time-resolved product distributions of the CO_2/O_2 plasma-based conversion reported in Fig. 4(b) show that compared to CO_2 plasma, CO_2/O_2 plasma increased the PE conversion rate and promoted higher liquid yields. The liquid yields per PE mass were 120.7% after 10 min for case J, 113.4% after 7.5 min for case K, and 115.3% after 7.5 min for case L, respectively.

The total gas yields per PE mass were 14.2%, 7.0%, and 11.9% for cases of J, K, and L, as also shown in Fig. 4(b). The corresponding gas selectivity and the yields of PE-derived gases are included in Fig. 2 to compare with the CO_2 plasma-based cases. The sum yields of H_2 and hydrocarbon gases were 1.0%, 0.9%, and 2.6% per PE mass for the three cases, suggesting CO_2/O_2 plasma can more effectively convert PE into liquid products than CO_2 plasma. CO was also the dominant gas with CO_2/O_2 plasma with the highest selectivity of 93%, as observed in case J.

PE bond cleavages were more intensive with CO_2/O_2 plasma than CO_2 plasma, leading to liquid products with narrower molecular weight distributions of shorter-carbon chain-length compounds (the results included in Table 2). CO_2/O_2 plasma also resulted in liquids with a higher degree of oxidation. The liquid oxygen content was 11.2% in case J, followed by 11.0% in case K and 9.8% in case J.
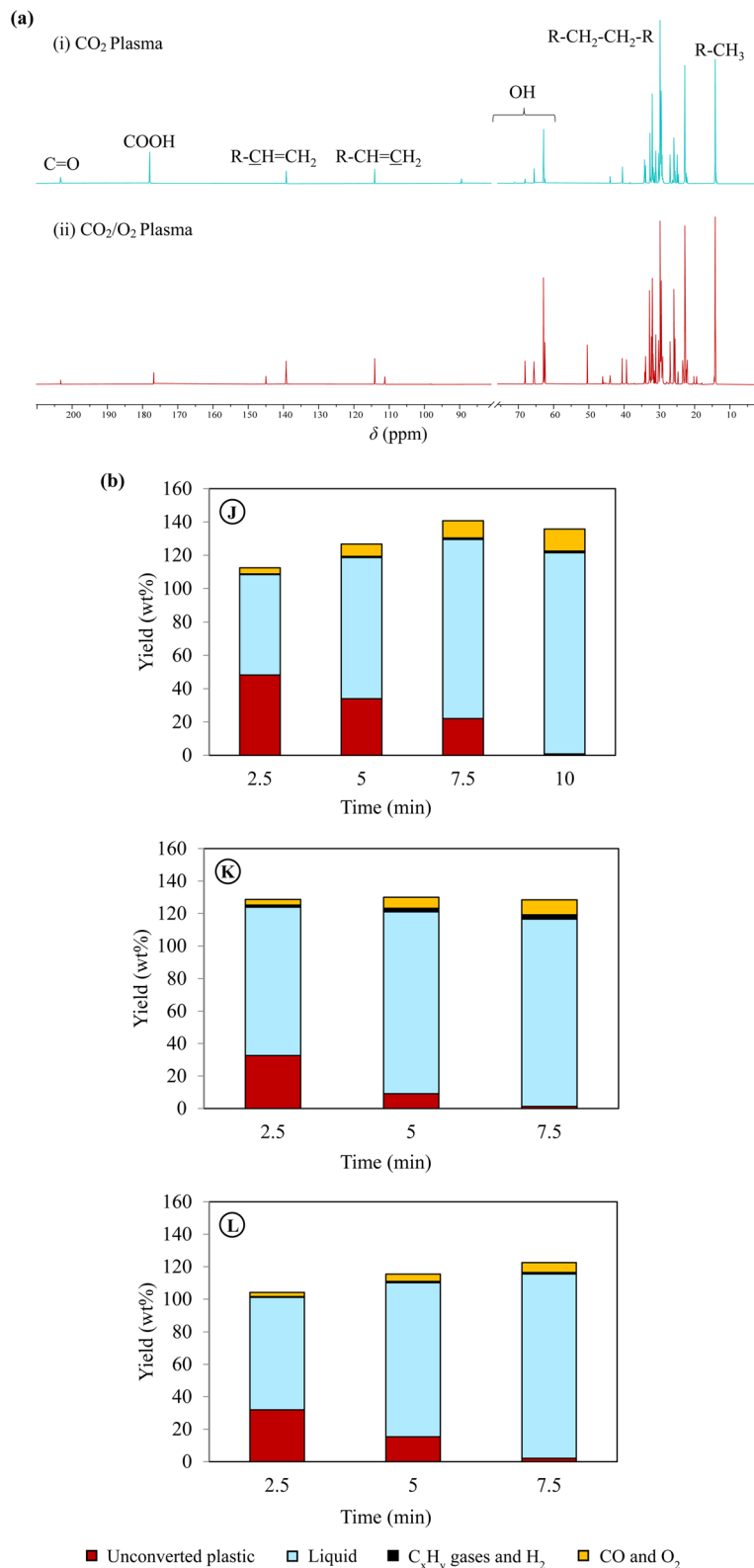
Fig. 4 Effect of oxygen addition on plasma co-upcycling of plastics and CO_2. (a) ^{13}C NMR spectra of liquid products obtained using (i) CO_2 plasma (case G), and (ii) CO_2/O_2 plasma (case J). The chloroform-d ($CDCl_3$) peak between chemical shifts 75 and 80 was hidden to improve the visibility of desired peaks, and (b) time-dependent product distribution during PE conversion using CO_2/O_2 plasma with different oxygen concentrations and gas residence times. Product characterizations can be found in Table 2 and Fig. 2, 3 for cases J, K and L.

The liquid compositions of the three CO_2/O_2 plasma cases are also included in Fig. 3 to compare with the CO_2 plasma-based liquids. The advantages of O_2 as a supplementary gas were not only limited to increasing the reaction rate of PE, producing higher yields of liquids with a higher degree of oxidation, and reducing molecular weights of the liquid products. Most importantly, employing CO_2/O_2 plasma caused a dramatic shift in product selectivity toward fatty alcohols. Case J was the optimal condition, producing the maximum fatty alcohol yield of 97.6% (or 80.9% per liquid). The fatty alcohols produced at this condition consisted of 49.7% of C_5–C_{12} alcohols, 44.1% of C_{13}–C_{28} alcohols, and 6.2% of C_{28}^+ alcohols. Among them, 12.7% were di-alcohols, and the rest were mono-alcohols. While products with other functional groups were reduced significantly, hydrocarbons in the liquid were only C_6–C_{10} paraffin and olefins. The shift in the product functional groups by CO_2/O_2 plasma was validated in the ^{13}C NMR result of the liquid (Fig. 4(a(ii))). In the NMR spectrum, OH, methyl, and methylene are the dominant peaks in the liquid produced using CO_2/O_2 plasma, suggesting a prevalence of mono-alcohol structures. The peaks of other oxygen-containing functional groups are minor due to their low concentrations. The ^{13}C NMR results-based quantification of the functional group selectivity (Table S4†), calculated using a method detailed in Section B of the ESI text,† agrees with the GC/MS-based results above, confirming that fatty alcohols were selectively produced by CO_2/O_2 plasma. Compared to case J, the alcohol yield was 86.9% (or 78.4% per liquid) in case K and 76.9% (66.7% per liquid) in case L. While selective production of fatty alcohols was confirmed in all CO_2/O_2 plasma cases, olefins and paraffin increased at longer residence time or higher O_2 concentrations. The oxygenated products were probably further deoxygenated under such conditions. Noteworthy, fatty alcohols in such high selectivity were not observed when PE was converted using air plasma. Although a high degree of oxygenation was also observed with air plasma, it only produced 51% fatty alcohols (Fig. S4†). Employing air plasma produced a much more complex mixture containing fatty alcohols, fatty acids, carbonyl, acetoxy esters, and ether functional group compounds.

2.3. Effect of PE on CO_2 conversion

In this plasma-based system, CO_2 was also converted by forming CO and oxidizing PE-derived hydrocarbons to produce oleochemicals. CO_2 conversion in the plasma reactor with and without PE for the different reaction conditions is compared in Fig. 5(a) to evaluate the effect of PE presence on CO_2 conversion. CO_2 conversion ranged from 2.9% to 4.9% when PE was absent, which is similar to CO_2 conversion using DBD plasma reactors reported in literature[36] (Fig. 5(b)). CO_2 conversion was always higher when PE was added (Fig. 5(a)), indicating that interactions between PE and CO_2 under plasma discharge can synergistically enhance CO_2 conversion. CO_2 conversion in case B was 6.3% with PE compared to 3.6% without PE. However, CO_2 conversion did not further increase by increasing the voltage in case C or frequency in case E, lowering the extent of synergistic increase in CO_2 conversion by PE. On the

other hand, increasing the gas retention time could further improve synergy. The highest CO_2 conversion of 7.5% was achieved in case G with PE, compared to 4.9% without PE. It also showed that the excessively high initial temperature reduces synergy. CO_2 conversions with and without PE were 4.0% and 3.5% for case I with the highest initial temperature of 400 °C. Overall, the synergistic increases of CO_2 conversion due to PE were positively correlated to the oxidation degree of the liquids. The most significant increase of CO_2 due to PE was observed in case G, which had the longest gas residence time, and delivered the highest yield of oleochemicals. CO_2/O_2 plasma slightly reduced CO_2 conversion compared to CO_2 plasma. The CO_2 conversion was 5.6% in case J and increased to 7.1% in case L with a longer gas residence time. On the other hand, CO_2 conversion was similar in cases J and K for different O_2 concentrations.

2.4. Mass balance of co-conversion system

PE, CO_2, and O_2 are all reactants in this plasma-based approach. The mass balances of the most promising conversions were reported: case G for CO_2 plasma and case J for CO_2/O_2 plasma. Mass closures of 96.9% and 98.6% were achieved when all reactants and quantified products were counted (Table S5†). In the case of CO_2 plasma, 75.9 g of PE and 24.1 g of CO_2 are converted to produce 46.4 g of fatty alcohols, 11 g of fatty acids, 10.5 g of olefins and 8.7 g of paraffin, assuming 100 g of converted feedstock PE and CO_2. Additionally, 12.1 g of CO and other minor gas products are produced. With CO_2/O_2 plasma, 72.6 g of PE, 17.6 g of CO_2, and 9.8 g of O_2 are converted to yield 70.9 g of fatty alcohols, 4.2 g of fatty acids, 8.5 g of olefins, 2.2 g of paraffin, and 9.6 g of CO. Sankey diagrams of the mass closures can be found in Fig. S6.†

2.5. Isotopic study-assisted reaction mechanisms

The plasma-based approach can effectively co-convert PE and CO_2 to produce commodity and platform chemicals in which CO_2 acts as the robust oxidant and cracking agent to depolymerize PE. In contrast, PE serves as a sink to insert CO_2 into its hydrocarbon chain. The formation of oxygenated hydrocarbons as the primary products and synergistic increase of CO_2 conversion together indicate strong interactions between PE and CO_2 under plasma discharge. When plasma discharge occurs to CO_2, electron collision impact generates radicals, ions, and other metastable particles of CO_2, CO, O, O_2, C, and many more.[36] However, the CO_2-derived particles can recombine, reducing the overall CO_2 conversion.[37,38] When PE is exposed to CO_2 plasma discharge, energetic electrons and active species of CO_2 plasma can attack the PE polymer chain to cleave its C–C and C–H bonds.[21,39] Not only does PE depolymerize, but the reactive CO_2 plasma species could further bond with the PE-derived hydrocarbons and hydrogen radicals.[40] This way, PE can act as a scavenger to inhibit the reverse reactions among CO_2 plasma species. The synergistic increase of CO_2 conversion by PE was pronounced with the longer gas residence time, implying that the chemical quenching effect was promoted by extending CO_2 and PE interactions
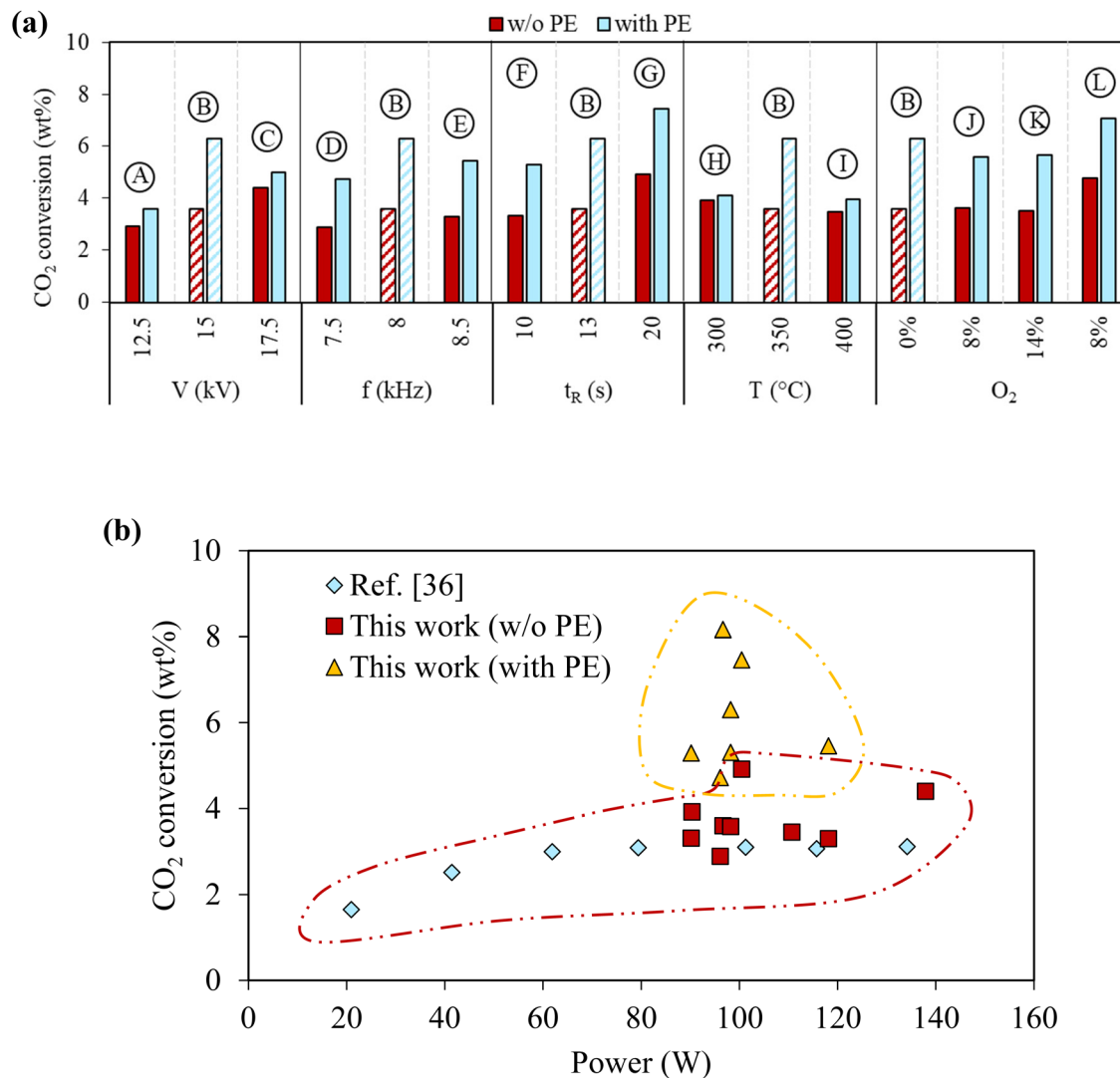
Fig. 5 Effect of PE on CO_2 conversion. (a) Cumulative CO_2 conversion after complete PE conversion under various reaction conditions, and (b) comparison of CO_2 conversion from this work with ref. 36 values.

under plasma discharge. In this work, we also found that doubling PE mass with the same CO_2 flow rate could increase CO_2 conversion from 6.3% to 8.2% for CO_2 plasma for case B, which can be explained by the increased scavenger (i.e., plastic) concentration inside the reactor.

Although plasma discharge forms a complex mixture and catalysts are absent in this study, the products displayed a high selectivity. The extensive optimization performed in this study suggests that multiple reactions involving different plasma species can be funneled down to the same type of products when the optimal reaction parameters are chosen. The interactions between CO_2 and PE were investigated by converting isotopic $^{13}CO_2$ and eicosane as a model compound of PE. The CO_2-originated C atoms in the compounds were tracked by analyzing the liquid product using GC/MS and comparing the mass-to-charge ratios (m/z) of the compounds resulting from the isotopic test with that of the corresponding standard

compounds. Despite $^{13}CO_2$ being more challenging to dissociate than regular CO_2,[41] ^{13}C carbons were successfully identified in the conversion products (see Fig. S7–S11, Tables S6, S7, and the ESI text, Section C† for a discussion of isotopic study).

The reaction mechanisms of PE and CO_2 co-conversion are proposed (Fig. 6). Under plasma discharge, electrons and metastable CO_2-derived plasma species (*e.g.*, CO_2, CO, O, O_2, C, C_2, and other C_xO_y) in the gas phase could attract PE to cleave its C–H and C–C bonds, forming the radicals of hydrogen and hydrocarbons (H, C_xH_y) with reduced chain lengths. The subsequent β-scission of the hydrocarbon radicals leads to alkenes and hydrogen radicals. Alternatively, the hydrocarbon radicals could also be saturated to form alkanes and alkenes by eqn (1) and (2), respectively. From the isotope results, CO_2-derived C atoms (up to 3 atoms) presented themselves in alkene products at their chain ends (Fig. S7†). Accordingly, the
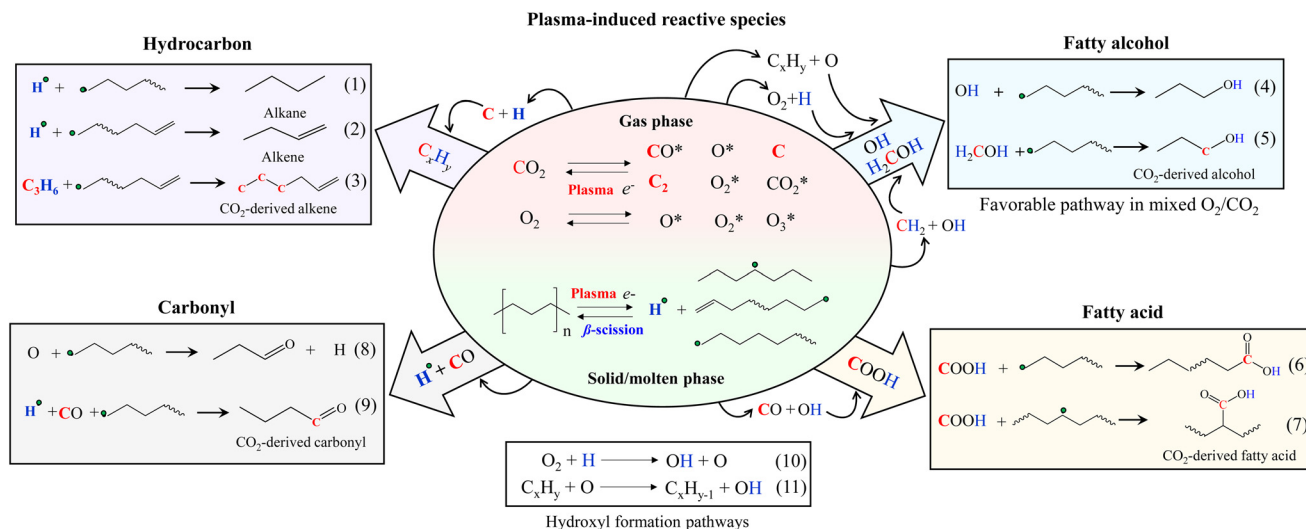
Fig. 6 Proposed reaction pathways of plasma-based co-upcycling of polyolefin and CO_2 with CO_2 or CO_2/O_2 plasma.

possible reaction pathway for CO_2-originated C atom to enter the alkene products can be a two-step process: (i) formation of C_xH_y radicals from CO_2-originated C and PE-derived H and (ii) further coupling reaction with hydrocarbon radicals (eqn (3)). Carbon coke formation was minor in this work because C further interacted with H or O.

PE-derived H and CO_2-derived O could form OH, which can further combine hydrocarbon radicals to produce fatty alcohols (eqn (4)). The CO_2-originated C atom linked to the OH in alcohols was also detected in the isotope results (Fig. S8†), suggesting the alcohol products can also form *via* with H_2COH intermediates containing CO_2-originated carbon[40,42,43] (eqn (5)). Although OH can combine with H to form water, this undesired reaction was not significant because the water content in the liquid products was negligible.

CO and OH can react with hydrocarbon radicals to form fatty acids (eqn (6) and (7)).[40,44] The metastable CO_2 and H could directly react with the hydrocarbon radicals to form the acids. However, this route has a much higher energy barrier than the previous route.[44,45] Carbonyl products are generated from O bonding with the hydrogen-abstracted hydrocarbon radicals (eqn (8)) or carbonylation reactions of CO with hydrocarbon radicals (eqn (9)). Our isotope results confirmed the CO_2-originated C atoms in carboxylic (COOH) (Fig. S9, S10 and Table S6†) and carbonyl (C=O) groups (Fig. S11 and Table S7†), which were in accordance with the reaction pathways shown in eqn (6) and (9), respectively.

Adding O_2 to CO_2 can affect the reaction rate, producing shorter carbon-chain molecules and shifting the product selectivity. Compared to CO_2, O_2 is easier to form plasma discharge to generate electrons and active species of O, O_2, and O_3.[37,38,46] Therefore, introducing a small amount of O_2 to CO_2 can increase the concentrations of energetic electrons and oxidative species in the system. CO_2/O_2 plasma resulted in the liquid with a lower carbon number distribution than CO_2

plasma, which can be explained by the stronger collision impact of CO_2/O_2 plasma that cleaves increased numbers of C–C and C–H bonds. Increased C–H bond scissions will also increase hydrogen radicals. Accordingly, the higher O and H concentrations in CO_2/O_2 plasma discharge (eqn (10) and (11)) compared to CO_2 plasma discharge will significantly increase OH formation,[46] promoting the alcohol-forming reactions (eqn (4) and (5)) and reducing hydrocarbon products. Fatty acids decreased considerably, possibly due to the reduced availability of the reactive CO intermediate species that suppress the reactions shown in eqn (6) and (7). Notably, CO_2 conversion was lower when PE was converted by CO_2/O_2 plasma than CO_2 plasma, suggesting the increased O in the system partially consumes CO_2-derived CO species to form CO_2. This increased combination reaction due to the added O_2 will reduce the PE-induced chemical quenching effect of CO_2 compared to PE conversion by CO_2 plasma. This statement was also supported in Fig. 5(a) result, as the extent of synergistic increase in CO_2 conversion was lower for CO_2/O_2 plasma. However, fewer CO species and higher OH concentration, paired with the scarcity of unbonded O species, combined with higher reactivity of OH-derived species,[47,48] resulted in the selective production of fatty alcohols under CO_2/O_2 plasma. If excess oxygen is supplied, the overwhelming presence of O species could introduce additional oxidative reactions, as found with air plasma. The enhanced collision impact by higher O_2 concentration may also promote secondary cracking reactions of the oxygenated hydrocarbons to increase hydrocarbons. Adding an optimal amount of O_2 to CO_2 during PE conversion could balance the reactions above, effectively controlling the product selectivity toward fatty alcohols without catalysts.

It should be emphasized that besides plasma gas composition, other reaction conditions also greatly impact reaction selectivity during the plasma-based co-conversion. Although the non-thermal plasma reactions do not need thermodynamic

equilibrium, the reactor gas temperatures strongly affect the reaction rate and oleochemical formation. There was an optimal temperature range that could promote the oxidation of PE. Higher degrees of oxidation were usually observed with an intermediate reactor temperature range around 350 °C. Temperatures higher than the optimal temperature increased the PE conversion rate, but it preferentially produced hydrocarbons than oleochemicals. For example, case I (T_i of 400 °C) had the highest average reactor temperature but produced mainly olefins and paraffins with the least oxygenated products. On the other hand, slower PE conversion rates and less oxidized products were observed with the reactor gas temperatures lower than the optimal temperature range. This observation suggests that product selectivity is determined by both chemical reactions and physical phenomena of feedstock and products. The plasma co-conversion of PE by activated CO_2 or CO_2 and O_2 involves multi-phase changes and reactions because the solid plastic changes to the molten/liquid phase and vapor/gas phase. A higher initial temperature or higher electricity voltage can promote strong plasma intensity. Activated CO_2 under such conditions can more easily attack PE for chain scissions, producing hydrocarbon molecules with shorter chain lengths. Higher initial temperatures and stronger plasma also raise overall reactor gas temperatures. At higher reactor temperatures, the produced hydrocarbons with smaller molecular weights would have sufficient volatility to evaporate from the molten/liquid phase. Once entrained in the gas stream, the hydrocarbon vapors and CO_2-derived species could quickly exit the reactor without sufficiently interacting with each other. This will increase hydrocarbons in the products and reduce oleochemical formation. Higher temperatures can also cause secondary cracking of oleochemicals to hydrocarbons. The reduced interaction between CO_2 and hydrocarbons would also hinder the chemical scavenger effect of PE to lower CO_2 conversion. On the other hand, lower reactor temperatures correspond to lower plasma intensity, which can reduce CO_2 conversion and, therefore, hinder PE depolymerization by activated CO_2. Under optimal reactor temperatures, activated CO_2 can depolymerize PE but the hydrocarbon products are unlikely to evaporate immediately at the reactor temperature conditions due to low volatilities. Thus, the hydrocarbons in their liquid phase could continue to react with CO_2 plasma species inside the reactor to produce oleochemicals. Increasing gas resistance time also significantly improved the oxygenated chemicals. The slower gas flow at the reactor inlet hinders the evaporation rate of the hydrocarbons and extends their residence time inside the reactor. This allows hydrocarbons to interact with CO_2-derived species more fully before products are swept away. While CO_2 or CO_2/O_2 plasma must depolymerize the polymer chain before the hydrocarbons are oxidatively functionalized, careful tuning of the reaction conditions and gas composition can balance polymer depolymerization, hydrocarbon volatilization, and the type of oxidation reactions to produce oleochemicals selectively. The chemical reactions and physical phenomena of plastic polymers and CO_2 under plasma discharge involving mass transfer in multi-phases warrant further investigation in future studies.

2.6. Conversion of common polyolefins and post-consumer mixed waste PE

Conversion of low-density PE (LDPE) and polypropylene (PP). The oxidative depolymerization by plasma-activated CO_2 or CO_2/O_2 mixture was also studied using other common polyolefins using the reaction conditions indicated in Table 1 for cases M to P. The compositions and elemental oxygen contents of the liquids derived from different types of plastics are given in Fig. 7(a). With CO_2 plasma, LDPE and PP produced 105.8% (case M) and 98.1% liquids (case N) containing 7.5% and 7.6% oxygen, respectively. The yields of fatty alcohols and fatty acids were 52.5% and 14.1% for LDPE and 49.5% and 12% for PP, respectively. When CO_2/O_2 plasma was employed, the liquid product yield and oxygen content were 113.5% and 11% for LDPE (case O) and 109.5% and 10.5% for PP (case P). These values are compared to 120.7% and 11.2% for the liquid obtained from PE (case G) using the same plasma reaction conditions. For both LDPE and PP, switching from CO_2 plasma to CO_2/O_2 plasma resulted in liquids with shorter carbon-chain compounds (the results are included in Table 2 to compare with other plastics). Because of the branched structure of LDPE and the abundance of less stable tertiary carbons in PP compared to the linear chain PE, the average molecular sizes of LDPE and PP-derived liquids were lower than that of the PE-derived liquid. For example, the total yield of C_5–C_{12} compounds was 64.4% for PE converted by CO_2/O_2 plasma (case G), whereas it was 76.7 and 66.8% for LDPE (case O) and PP (case P). Similar to what was observed with PE, fatty alcohols became the dominant products when LDPE and PP were converted by CO_2/O_2 plasma. The fatty alcohol yield was 87.8% (77.4% of liquid) for LDPE and 81.3% (74.2% of liquid) for PP. ^{13}C-NMR spectra of the liquids (Fig. S12†) and the NMR-based product selectivity (Table S8†) also confirm the selectivity production of fatty alcohols by CO_2/O_2 plasma.

Conversion of mixed waste plastics. The applicability of the plasma-based conversion system on real-world waste plastics with impurities was investigated using multi-colored and mixed post-consumer PE (PC-PE) collected from a material recovery facility rejected waste bale designated for landfills. The PC-PE was washed and sized before use (Fig. S13†). The reaction conditions are shown in Table 1 (cases Q and R). The time-resolved product distribution is given in Fig. S14(a),† and gas selectivity and CO_2 conversion can be found in Fig. S14(b).† In addition to liquid and gas products, there were about 2% solid residues due to the impurity content in PC-PE. The liquid yield from PC-PE was 104.4% with CO_2 plasma (case Q) and 111.5% with CO_2/O_2 plasma (case R), both achieved after 10 min. Compared to PE, the liquid products of PC-PE had slightly narrower molecular weight distributions (the results included in Table 2). The oxygen content in the liquids was 7.1% with CO_2 plasma and 10.9% with CO_2/O_2 plasma, comparable to the PE-derived liquids. The liquid compositions can be found in Fig. 7(a), along with other plastic-
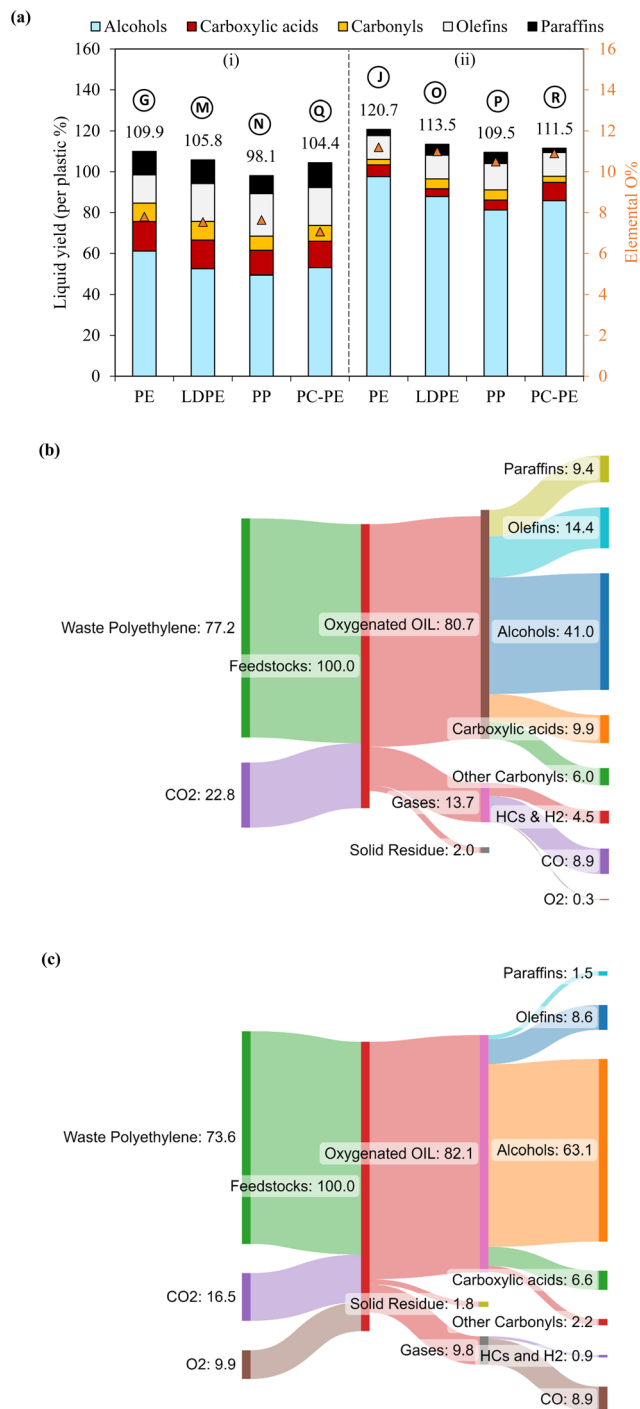
Fig. 7 Plasma-based upcycling of common polyolefins and post-consumer mixed PE. (a) Liquid product composition from conversion of PE, LDPE, PP and PC-PE by (i) CO_2 and (ii) CO_2/O_2 plasma, (b) overall mass balance from PC-PE conversion by CO_2 plasma, and (c) overall mass balance from PC-PE conversion by CO_2/O_2 plasma.

derived liquids. Oxygenated compounds with a total yield of 73.7% were obtained from PC-PE using CO_2 plasma, which included 53.1% of fatty alcohols, 12.9% of fatty acids, and 7.7% of carbonyls. Fatty alcohols were the dominant products

with CO_2/O_2 plasma, yielding 85.8% (76.9% of liquid). The fatty alcohols were mostly $<C_{28}$ compounds (the results included in Table 2), similar to the PE-derived liquid. CO_2 conversion during co-conversion with PC-PE was 7.5% for CO_2 plasma and 4.1% for CO_2/O_2 plasma.

Sankey diagrams of the PC-PE conversion systems using CO_2 plasma and CO_2/O_2 plasma are shown in Fig. 7(b), with 96.8% and 93.7% of mass closures (given in Table S7†). In the case of CO_2 plasma, 77.2 g of PC-PE and 22.8 g of CO_2 are converted to produce 41 g of fatty alcohols, 9.9 g of fatty acids, 6 g of carbonyls, 14.4 g of olefins and 9.4 g of paraffin, assuming 100 g of converted feedstock PC-PE and CO_2. Additionally, it produces 8.9 g of CO and 4.5 g of H_2 and hydrocarbon gases. When CO_2/O_2 plasma is employed, 73.6 g of PC-PE, 16.5 g of CO_2, and 9.9 g of O_2 are converted to produce 63.1 g of fatty alcohols, 6.6 g of fatty acids, 8.6 g of olefins, and 8.9 g of CO gas. These results show the presented approach can be applied to waste polyolefin plastics.

2.7. TEA and LCA

The presented approach can convert waste plastics and CO_2 mixtures into highly desired oleochemicals and syngas-like products in a single step without catalysts or other costly co-agents. Notably, current chemical recycling technologies such as pyrolysis of polyolefins only produce low-quality hydrocarbon fuels requiring catalytic upgrading to chemicals.[31,49,50] The economic and environmental impact of commercializing the plasma-based conversion of waste plastics and CO_2 is evaluated based on the experimental results of PC-PE conversion, specifically, case Q (CO_2 plasma) and case R (CO_2/O_2 plasma). Fig. 8(a) shows a simplified block diagram for a commercial-scale plasma-based waste plastic to fuels and chemicals facility. The plasma decomposition of PC-PE yields light gases and liquid products. The liquid products contain olefins, paraffin, fatty alcohols, fatty acids, and carbonyls, and the gases consist of CO, H_2, and C_1–C_5 hydrocarbons. Multiple fractional distillation and distillation columns were utilized to separate the compounds based on their boiling points, and the gases were combusted to generate power and heat to meet the facility's energy requirements. The material and energy flows of the 200 metric tons per day (MTPD) facility are presented in Fig. S18 and S19.† A 200 MTPD PE waste plasma facility produces 98–142 TPD of fatty alcohols, 24–19 TPD of fatty acids, 37–22 TPD of olefins, 24–4 TPD of paraffin, 15–7 TPD of carbonyls for case Q and case R respectively. The annual processing capacity of the plasma-based waste plastic conversion plant represents 0.29% of the total PE waste produced in the United States in 2019.[51]

The facility processes waste plastic collected for $25 per metric ton (MT), including transportation and pretreatment, which is consistent with previous TEA studies on waste PE thermochemical conversion.[8,52] The PE waste considered in this study cannot be mechanically recycled and is routinely landfilled. Material recovery facilities in the US collect raw waste with a tipping fee of up to $50 per MT, representing a significant revenue source.[53,54] The plastic fraction can be sep-
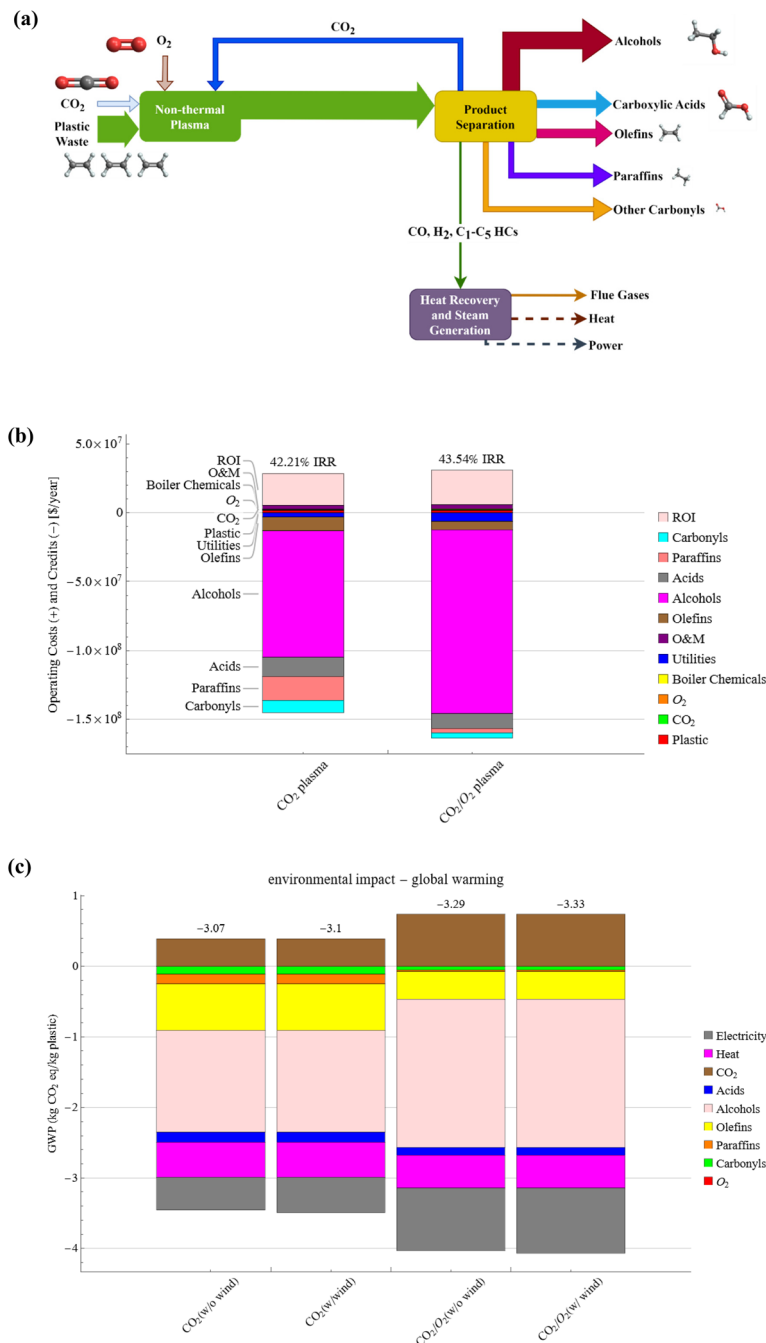
Fig. 8 TEA and LCA for the plasma-based conversion process. (a) Simplified block flow diagram for plasma-based plastic waste to fuels and chemicals, (b) operating costs and internal rates of return for a commercial-scale plasma-based waste plastic to fuels and chemicals facility, and (c) global warming potential (GWP) for a commercial-scale plasma-based waste plastic to fuels and chemicals facility using on-site power production or wind electricity.

arated and pretreated to remove impurities that impact the conversion performance and quality of the plasma process, which increases the value of the plastic waste to $25 per MT. According to the US Billion Ton report of 2023, the price per MT of CO_2 ranges from $30–$200 depending on the source and the purity of the CO_2 stream.[55] The study assumed a standard cost of $35 per MT of CO_2, consistent with prior studies

on CO_2 utilization processes.[56,57] Sensitivity analysis is conducted to evaluate the importance of the plastic and CO_2 stream price in the plant's economics. The plasma-based conversion of waste plastic and CO_2 generates multiple chemicals, and the on-site combustion of the gases produces surplus power and heat that are sold to the grid. The average market price of the products was obtained from online databases and

documented in Table S10.† [27,28,58–60] The average price of fatty alcohol and fatty acids is $2.82 per kg and $1.79 per kg, respectively, and the average price of the other chemicals ranges from $0.83 to $2.19 per kg.

The estimated total installed equipment cost (TIC) breakdown for a 200 MT per day plastic waste facility is presented in Fig. S20.† The TIC for PC-PE/CO_2 plasma and PC-PE/CO_2/O_2 plasma is $52.7 million and $56.9 million, respectively. At a Lang factor of 5, the capital cost ranges from $188–202 million. The plasma reactor and heat recovery and steam generation (HRSG) systems are the most expensive pieces of equipment, representing over 85% of TIC in both cases.

The internal rate of return (IRR) and net present value (NPV) were determined from the discounted cash flow analysis to assess the economic performance of the facilities. The financial parameters used in the TEA are presented in Table S9.† The cash flow result is shown in Fig. 8(b). The IRR and NPV are 42.2% and 739.6 $MM, respectively, for the CO_2 plasma-based facility, and 43.5% and 854.2 $MM for the CO_2/O_2 plasma-based facility. The latter has a higher IRR because of the high alcohol yield, generating considerable revenue.

The minimum selling price (MSP) is not a primary economic indicator in this study, but it was calculated to provide a comparison of the chemical products of this process with current petroleum processes. The MSP of the product with the highest yield in each scenario was estimated, and the sale of the co-products contributed to the revenue in estimating the MSP. The MSP of the primary product was calculated from the discounted cash flow, assuming an internal rate of return of 10% over a 20-year lifespan of the plant. In both cases, fatty alcohols were selected as the primary product. The CO_2 plasma-based approach has an MSP of $-0.59 per kg, while the CO_2/O_2 plasma-based approach has an MSP of $0.14 per kg for fatty alcohols. The MSP calculated for both cases is significantly lower than the market price of fatty alcohols ($2.82 per kg). The negative MSP for the CO_2 plasma-based facility indicates that the other chemical products (acids, paraffin, olefins and carbonyls) generate sufficient revenue for the NPV to remain positive. Fig. S21† displays the contributions of the co-product revenues and operating expenses on the MSP of fatty alcohol for each scenario.

Sensitivity analysis was carried out to assess the effect of different process variables on the net present value in each scenario. The profitability of the plant heavily depends on the product's sales, which are solely determined by market dynamics. Throughout a plant's lifespan, economic conditions can vary. Sensitivity was determined in a ±20% variation in the baseline cost of capital investment, feedstock prices, plasma energy, and product prices, as shown in Fig. S22.† The sensitivity results indicate that the capital cost and fatty alcohol price are the most significant determinants of the NPV. The plastic price, CO_2 price, and plasma energy consumption have a limited impact on the NPV.

This study utilized LCA to evaluate the environmental impact of producing chemicals from the non-thermal plasma deconstruction of plastic waste. As mentioned above, electricity and heat are generated from the combustion of gases and heavy compounds to cover the plant's energy requirement, and the surplus is injected into the grid, which accounts for displacement credits. In the analysis, we consider additional scenarios where the facility energy requirements are supplied by wind energy, and the total on-site energy generation displaces grid power. Furthermore, we assumed all the products substitute similar products from fossil-based processes, resulting in credits earned. The life cycle inventory is available in Table S11.†

LCA results are presented in Fig. 8(c) and show that the process has net negative global warming potentials (GWP) of −3.07 and −3.29 kg CO_{2e} per kg of plastic for PC-PE/CO_2 plasma and PC-PE/CO_2/O_2 plasma, respectively. The GWP of the scenarios with wind energy is slightly lower. The negative emissions indicate that the process results in an overall reduction of emissions in the carbon economy. This occurs because of the displacement of sourced fossil chemicals and fuels. The main positive contributor that increases GWP in the process is the carbon emissions produced from the on-site combustion of flue gases in the power generation unit. However, the product credits from chemicals, fuels, excess heat, and power exceed the emissions. Sensitivity analysis indicates that fatty alcohol, olefins, process heat, and electricity impact GWP most, and the results are shown in Fig. S23.† Carbonyls and paraffin have a relatively low impact on the GWP due to their low yields. Table S12† shows the results for all TRACI environmental impact categories, including eutrophication, ecotoxicity, and others.

3. Conclusion

The study effectively demonstrates the potential of non-thermal plasma-activated CO_2/O_2 technology for upcycling plastic waste into oleochemicals. During their plasma-based process, CO_2 and plastic conversions were synergistically enhanced. Using O_2 as a supplementary gas was a highly effective and simple approach to tailor chemical selectivity toward fatty alcohols and increase product yield.

The 200 MTPD waste plastic facility produces 32 524 MT and 47 286 MT per year of fatty alcohol for the CO_2 and CO_2/O_2 plasma-based facility, respectively. This represents ~2.4% of the global market demand for fatty alcohol in 2019.[61] TEA results indicate a promising IRR for the proposed process, underlining its economic viability as an alternative to conventional recycling and waste management methods. The analysis further suggests a negative GWP due to the avoided emissions of the various products. This GWP compares favorably to existing waste management practices, emphasizing the environmental benefits of this innovative approach. Our evaluation across different scenarios, varying in feedstock compositions, reaffirmed the robustness and flexibility of the plasma-based technology. The sensitivity analysis further highlighted the significant impact of the fatty alcohol yield, which not only

impacts the process economics but also the GHG emissions. The viability of this technology highly depends on the yield of the products, particularly fatty alcohol. Therefore, enhancing the process selectivity of alcohols will significantly increase the economic and environmental benefits of plasma-based technology.

The research opens avenues for future exploration, notably in optimizing process conditions, scaling up the technology for industrial application, and exploring the integration of renewable energy sources to reduce the GWP further. Additionally, investigating the feasibility of other value-added products from plastic waste using non-thermal plasma could expand the economic and environmental benefits of this promising technology.

Future work should also focus on detailed environmental impact assessments, exploring partnerships with waste management and recycling industries, and conducting pilot studies to validate the TEA presented. This would provide a comprehensive understanding of the technology's practical implications and facilitate the global transition towards more sustainable waste management practices.

4. Experimental

4.1. Materials

High-density polyethylene (PE or HDPE; $M_w \sim 60\,000$ Da) and polypropylene (PP; $M_w \sim 200\,000$ Da) were purchased from Yangli Tech Company (China), and low-density (LDPE; $M_w \sim 80\,000$ Da) were procured from DOW Chemicals. The colored and mixed post-consumer polyethylene (PC-PE; $\sim75\,000$ Da) was collected from material recovery facilities. All HPLC-grade solvents (dichloromethane, toluene, pyridine, and tetrahydrofuran) were purchased from Fisher Scientific. High-purity GC carrier gases were purchased from Airgas. The silylation agent (N,O-bis(trimethylsilyl)trifluoroacetamide with trimethylchlorosilane) for identification of carboxylic acid and alcohols compounds, and NMR relaxation agent (chromium(III) acetylacetonate) were supplied by Sigma Aldrich. High-purity standard gases (CO, CO_2, H_2, O_2) and light hydrocarbon gases were purchased from Praxair. Isotopic $^{13}CO_2$ was supplied by Cambridge Isotope Laboratories, Inc. The standard chemicals of alkanes (C_6–C_{40}), alkenes (C_5–C_{23}), dienes (C_6–C_{14}), alcohols (C_6–C_{30}), carboxylic acids (C_6–C_{24}) and carbonyl (C_6–C_{18}) compounds used for the GCMS calibration were purchased from Fischer Scientific, Thermo Scientific, TCI America, and Sigma Aldrich. A detailed list of the standard chemicals and their sources is provided in Section A of the ESI text.†

4.2. Plasma-based plastics conversion process

Fig. S1† shows a schematic diagram of the plasma reactor and product recovery system. The experiments were conducted in a co-axial dielectric barrier discharge (DBD) reactor made of quartz. A tungsten rod was inserted as a high-voltage electrode. The outer surface of the reactor was covered by a copper sheet, which acted as a grounded electrode, and was insulated. The high-voltage electrode was connected to a high-voltage AC power supply (Nanjing Suman Company, CTP-2000 K), with a maximum peak-to-peak sinusoidal voltage of 30 kV and a center frequency of 10 kHz. Electric voltage and current were measured using a high-voltage probe (i.e., P6015A from Tektronix) and a high-response current probe (Pearson Electronics, Inc., Pearson 2877) equipped with an oscilloscope (Tektronix MDO3102 mixed domain). About 0.15 g of plastics was placed inside the plasma reactor. Reaction gases entered the reactor at the inlet. The volume flow rates were controlled by volumetric flowmeters, calibrated prior to the experiments by a high-accuracy universal flow controller (Agilent, model ADM G6691) with an accuracy of ±0.2 mL min^{-1}. The gas flow rate was between 32.5 and 65 mL min^{-1}. When external heating was required, the reactor was heated by a coil heater.

Initially, the reactor was heated externally until the internal reactor gas temperature reached the preset temperatures. Later, the heater was turned off before the plasma generator was turned on. The reaction was carried out under atmospheric pressure, and reaction time was calculated from when the plasma generator was turned on. The vapors and gases leaving the reactor at the other end were passed through a two-stage condenser cooled with methanol–dry ice mixtures to collect liquids and non-condensable gases were sent to an online micro-GC for gas analysis. During the reaction, the reactor outlet gas flow was continuously measured downstream of the condenser using the high-accuracy universal gas flowmeter. The reactor gas temperature was measured, and the recorded current and voltage were used to determine plasma power. The masses of the solid residues and liquids were determined by weighting the reactor and the condenser before and after the conversion using an analytical balance with an accuracy of 0.0001 g (Veritas, M124AS).

For converting eicosane using isotopic $^{13}CO_2$ plasma, the experiment was carried out using a DBD plasma reactor. The reactor had similar dimensions to the above-mentioned plasma reactor, except it had inlet and exit valves. Plasma discharge was generated in the reactor with closed values containing about 0.15 g of eicosane and $^{13}CO_2$ gas. After conversion, the products were collected from the reactor by dissolving in a mixture of toluene and pyridine solvents (2.5/1.5, v/v). Eicosane was also converted in the same reactor using regular CO_2 as plasma gas to collect products, aiding product identification during the isotopic tests.

Definitions for product yield, selectivity, and energy efficiency

Liquid or solid yields based on the initial plastic mass are calculated as shown below:

$$\text{Liquid yield}\,(\%) = \frac{\text{Mass of liquid product}}{\text{Plastic feedstock mass}} \times 100\%$$

$$\text{Soild yield}\,(\%) = \frac{\text{Mass of solid residue}}{\text{Plastic feedstock mass}} \times 100\%.$$

The mass yield of an individual gas compound per plastics are calculated as:

$$\text{Gas compound yield}\ (\%) = \frac{\text{Mass of the gas compound}}{\text{Plastic feedstock mass}} \times 100\%$$

where gas compound mass was calculated using the following equation:

Mass of a gas compound
$$= \text{Mass fraction of the gas} \times \text{total mass of all gas products.}$$

The mass selectivity of individual gas compound among the total gas product was calculated as:

$$\text{Gas compound selectivity}\ (\%) = \frac{\text{Mass of an individual gas}}{\text{Total mass of the gas product}} \times 100\%.$$

The yield of an individual liquid compound per initial plastic mass is calculated as:

$$\text{Liquid compound yield}\ (\%) = \frac{\text{Mass of a compound}}{\text{Plastic feedstock mass}} \times 100\%.$$

The mass selectivity of a compound with a functional group in the liquid is calculated as:

Compound selectivity in liquid $(\%)$
$$= \frac{\text{Mass of the compounds with a functional group}}{\text{Total mass of the liquid product}} \times 100\%.$$

CO_2 conversion is calculated as:

CO_2 conversion $(\%)$
$$= \frac{\text{Total input } CO_2 \text{ mass} - \text{total output } CO_2 \text{ mass}}{\text{Total input } CO_2 \text{ mass}} \times 100\%.$$

For mass balance of the conversion system including all reactants, the calculations are given below:

Product yield $(\%)$
$$= \frac{\text{Mass of the product}}{\text{Combined mass of the plastic and converted } CO_2 \text{ (and } O_2)} \times 100\%.$$

4.3. Characterization methods

High-temperature gas chromatography with mass spectrometry and flame ionization detector (HT-GC/MS-FID). Liquid products dissolved in the toluene and pyridine solvent mixture were analyzed using HT-GC/MS-FID. Before analysis, the samples were derivatized by adding 200 μL of the BSTFA silylation agent to 3 mL of the solution and agitated for 60 min at 60 °C. In this GC system (Agilent 7890B) with MS (MS 5977A, Agilent, USA) and FID, two high-temperature columns (400 °C, Phenomenex ZB-5HTs, 60 m × 250 μm × 0.25 μm) were used. The GC oven temperature was initially kept at 40 °C for 3 min, increased to 400 °C with a heating rate of 3 °C min^{-1}, and held at 400 °C for another 5 min. The GC/MS was also configured with a Polyarc reactor (Polyarc System, Activated Research Technologies, Inc., USA) in the front of the FID to provide a carbon mass-based response for the detected analytes irrespective of their functional group or boiling point. The helium gas flow rate in the columns was 1 mL min^{-1}, and the split ratio at the GC inlet was 20 : 1. The temperature of the FID detector was set at 375 °C. Agilent MassHunter software was used to process the GC chromatograms and measure peak areas. The compounds in the liquid products were identified using a combination of tools, including the NIST MS spectral and mass ion database. High-purity standards of alkane, alkene, alcohol, diol, carboxylic acid, and aldehyde were injected into the GC to aid MS identification. Five different concentrations of the alkane standards were injected to calibrate the Polyarc-FID for liquid product quantification. Since the Polyarc-FID calibration is based on carbon response, the calibration factor from a particular carbon number of alkane can be used for any compound containing the same number of carbons. The resultant calibration curves had regression coefficients higher than 0.99. Unless specified otherwise, the mass selectivity and yields of individual liquid compounds or a specific functional group in the liquid product are from GC analysis.

Individual products up to C_{28} carbon number could be quantified using the Polyarc-FID due to their good peak separations in the MS chromatograms. In the $>C_{28}$ compound region, co-elution of different class compound peaks was noticed in some liquid samples for higher molecular weight products. In these limited cases, the functional group selectivity of compounds up to C_{28} was considered for the entire liquid product.

Gas analysis. The gas products were analyzed online using the Varian CP4900 micro-GC system (Varian, Inc., now owned by Agilent Technologies). In the GC oven, four different columns were connected to four different thermal conductivity detectors (TCD). The first TCD quantifying H_2, CH_4, CO, and O_2 used argon as a carrier gas, while the rest of the TCDs quantifying CO_2 and other light hydrocarbons used helium as a carrier gas. The GC was pre-calibrated by injecting different volumes of the standard gas mixtures. Compass CDS software (Scion Instruments, UK) was used to operate, calibrate, and quantify the gaseous compounds. The gas product concentrations (v/v) were calculated using the calibration curves and the peak areas of the corresponding compound in TCD. The outlet flow rate of the reactor during the plasma conversion was used to measure the total gas product volume. The total gas product volume and individual gas concentrations (v/v) were then used to calculate the total mass of the inlet gas.

Elemental analysis. Elemental analyses of the plastic feedstock and liquid products were performed using standard procedure in Elementar, vario MICRO cube (Elementar, Hanau, Germany) elemental analyzer and were triplicated. The element contents of C, H, N, and S were measured, while the oxygen content was calculated by subtracting C, H, N, and S contents from the total content.

Karl Fischer analysis. Water content in liquid products was measured using a Volumetric Karl Fischer titrator (Mettler Toledo, model V30S) following the ASTM E203 Standard.

About 0.04–0.06 g of samples were dissolved in 1 mL of Hydranal solvent (dry methanol), and the averages of triplicate measurements were reported.

Nuclear magnetic resonance (NMR). [13]C nuclear magnetic resonance (NMR) experiments for liquid samples were performed using an Avance NEO-400 spectrometer. The NMR samples were prepared by adding 0.2 g of samples in 1 mL of chloroform-D solvent and a relaxation agent, 3 M chromium (III) acetylacetonate, to improve the intensity of weak signals.[63] The sample mixtures were ultrasonicated for an hour before analysis. The ^{13}C NMR spectra were acquired using pulse sequence "zgig" at 25 °C with a relaxation delay of 2 seconds and 7200 scans over a total acquisition time of around 7 hours. Spectral width and central frequency were 248 ppm and 100 ppm, respectively. The NEO-400 is operated using Topspin 4.0 software, and the NMR spectra were processed using MestReNova v14.3 software. The NMR peaks were assigned based on literature.[62–64]

4.4. TEA

TEA was conducted to evaluate the commercialization potential of a plasma-based plastic waste to chemicals and fuel facility. The facility capacity was modeled as a 200 MT per day unit capable of processing plastic waste streams from multiple material recovery facilities.[53] The TEA includes a detailed process design described in Fig. S15.† Rigorous material and energy balance calculations were conducted using the US DOE-funded BioSTEAM chemical process modeling package.[65] Equipment costs and financial assumptions are based on the NREL report by Humbird et al.[66] Material and utility costs are based on historical market price data. NPV and IRR were calculated based on a 20-year project lifetime. The process generates multiple products, so the primary comparison metric is the IRR instead of the MSP. However, the MSP of the product with the highest yield in the process was calculated. More information on the TEA methodology is provided in Section D of the ESI text.†

4.5. LCA

LCA was developed to estimate the GWP and other environmental impact factors of the process. The LCA was performed in OpenLCA 1.11.0.67 The Ecoinvent version 3.7 database and the Tool for Reduction and Assessment of Chemicals and Other Environmental Impacts (TRACI) were used to calculate the ecotoxicity, acidification, eutrophication, global warming, ozone depletion, photochemical oxidation, and carcinogenic impacts of the process. The impact allocation methodology is the system expansion or displacement method. The functional unit is a kg of waste plastic. The system boundary is described in Fig. S17,† and consists of a cradle-to-factory gate recycling analysis. Plastic is received as a material with no environmental burden. The TEA and LCA analyses include sensitivity analysis of key technical, economic, and environmental impact parameters. More information on the lifecycle assessment methodology is provided in Section D of the ESI text.†

Data availability

All data needed to evaluate this work are available in the main manuscript and/or the ESI.†

Conflicts of interest

X. B., L. A, and H. R. have filed US Patent Application 18/451,482 with the support of the Iowa State University Research Foundation. All other authors declare no competing interests.

Acknowledgements

References

1 H. Li, H. A. Aguirre-Villegas and R. D. Allen, Expanding plastics recycling technologies: chemical aspects, technology status and challenges, *Green Chem.*, 2022, **24**, 8899–9002.

2 R. Geyer, J. R. Jambeck and K. L. Law, Production, use, and fate of all plastics ever made, *Sci. Adv.*, 2017, **3**, e1700782.

3 Statista, Plastic Production Worldwide, 2021, available at: **https://www.statista.com/statistics/282732/global-production-of-plastics-since-1950/**, accessed October 20, 2023.

4 Y. Chen, A. K. Awasthi, F. Wei, Q. Tan and J. Li, Single-use plastics: Production, usage, disposal, and adverse impacts, *Sci. Total Environ.*, 2021, **752**, 141772.

5 U.S. Environmental Protection Agency, Plastics: Material-Specific Data, available at: **https://www.epa.gov/facts-and-figures-about-materials-waste-and-recycling/plastics-material-specific-data**, accessed October 20, 2023.

6 X. Zhao, M. Korey and K. Li, Plastic waste upcycling toward a circular economy, *Chem. Eng. J.*, 2022, **428**, 131928.

7 P. J. Woolcock and R. C. Brown, A review of cleaning technologies for biomass-derived syngas, *Biomass Bioenergy*, 2013, **52**, 54–84.

8 O. Olafasakin, J. Ma, V. Zavala, R. C. Brown, G. W. Huber and M. Mba-Wright, Comparative Techno-economic Analysis and Life Cycle Assessment of Producing High-Value Chemicals and Fuels from Waste Plastic via Conventional Pyrolysis and Thermal Oxo-degradation, *Energy Fuels*, 2023, **37**, 15832–15842.

9 H. M. Nguyen and M. L. Carreon, Non-thermal Plasma-Assisted Deconstruction of High-Density Polyethylene to Hydrogen and Light Hydrocarbons over Hollow ZSM-5

Microspheres, *ACS Sustainable Chem. Eng.*, 2022, **10**, 9480–9491.

10 A. Bogaerts and E. C. Neyts, Plasma Technology: An Emerging Technology for Energy Storage, *ACS Energy Lett.*, 2018, **3**, 1013–1027.

11 B. Tabu, K. Akers and P. Yu, Non-thermal atmospheric plasma reactors for hydrogen production from low-density polyethylene, *Int. J. Hydrogen Energy*, 2022, **47**, 39743–39757.

12 C. Ducharme, N. J. Themelis and M. J. Castaldi, *Technical and Economic Analysis of Plasma-assisted Waste-to-Energy processes*, 2010.

13 T. Maczka, M. Wnukowski, E. Sliwka and L. Niedzwiecki, *Pilot Installation for the Thermal Plasma Treatment of Plastic Wastes*, 2013.

14 S. Kwon and S. k. Im, Feasibility of non-thermal plasma gasification for a waste-to-energy power plant, *Energy Convers. Manage.*, 2022, **251**, 114978.

15 A. Lusi, H. Hu and X. Bai, Producing high yield of levoglucosan by pyrolyzing nonthermal plasma-pretreated cellulose, *Green Chem.*, 2020, **22**, 2036–2048.

16 A. Lusi, H. Radhakrishnan, H. Hu and X. Bai, Plasma electrolysis of cellulose in polar aprotic solvents for production of levoglucosenone, *Green Chem.*, 2020, **22**, 7871–7883.

17 A. Lusi, H. Radhakrishnan, H. Hu and X. Bai, One-pot production of oxygenated monomers and selectively oxidized lignin from biomass based on plasma electrolysis, *Green Chem.*, 2021, **23**, 9109–9125.

18 I. Aminu, M. A. Nahil and P. T. Williams, Hydrogen from Waste Plastics by Two-Stage Pyrolysis/Low-Temperature Plasma Catalytic Processing, *Energy Fuels*, 2020, **34**, 11679–11689.

19 L. Yao, J. King, D. Wu, S. S. C. Chuang and Z. Peng, Non-thermal plasma-assisted hydrogenolysis of polyethylene to light hydrocarbons, *Catal. Commun.*, 2021, **150**, 106274.

20 I. Aminu, M. A. Nahil and P. T. Williams, Hydrogen Production by Pyrolysis–Nonthermal Plasma/Catalytic Reforming of Waste Plastic over Different Catalyst Support Materials, *Energy Fuels*, 2022, **36**, 3788–3801.

21 L. S. Diaz-Silvarrey, K. Zhang and A. N. Phan, Monomer recovery through advanced pyrolysis of waste high density polyethylene (HDPE), *Green Chem.*, 2018, **20**, 1813–1823.

22 A. George, B. Shen and M. Craven, A Review of Non-Thermal Plasma Technology: A novel solution for CO_2 conversion and utilization, *Renewable Sustainable Energy Rev.*, 2021, **135**, 109702.

23 Grand View Research, Oleochemicals Market Size, available at: **https://www.grandviewresearch.com/industry-analysis/oleochemicals-industry**, accessed November 10, 2023.

24 P. Munkajohnpong, C. Kesornpun, S. Buttranon, J. Jaroensuk, N. Weeranoppanant and P. Chaiyen, Fatty alcohol production: an opportunity of bioprocess, *Biofuels, Bioprod. Biorefin.*, 2020, **14**, 986–1009.

25 H. A. Wittcoff, B. G. Reuben and J. S. Plotkin, *Industrial Organic Chemicals*, John Wiley & Sons, 2012.

26 J. Salimon, N. Salih and E. Yousif, Industrial development and applications of plant oils and their biobased oleochemicals, *Arabian J. Chem.*, 2012, **5**, 135–145.

27 ChemAnalyst, Fatty Alcohol Price Trend and Forecast, available at: **https://www.chemanalyst.com/Pricing-data/fatty-alcohol-1084**, accessed November 10, 2023.

28 ChemAnalyst, Fatty Acid Price Trend and Forecast, available at: **https://www.chemanalyst.com/Pricing-data/fatty-acid-1257**, accessed November 10, 2023.

29 J. Shah, E. Arslan, J. Cirucci, J. O'Brien and D. Moss, Comparison of Oleo- vs Petro-Sourcing of Fatty Alcohols via Cradle-to-Gate Life Cycle Assessment, *J. Surfactants Deterg.*, 2016, **19**, 1333–1351.

30 C. Liang, U. R. Gracida-Alvarez, T. R. Hawkins and J. B. Dunn, Lifecycle Assessment of Biochemicals with Clear Near-Term Market Potential, *ACS Sustainable Chem. Eng.*, 2023, **11**, 2773–2783.

31 H. Li, J. Wu and Z. Jiang, Hydroformylation of pyrolysis oils to aldehydes and alcohols from polyolefin waste, *Science*, 2023, **381**, 660–666.

32 Y. Zhang, Z. Fu, W. Wang, G. Ji, M. Zhao and A. Li, Kinetics, Product Evolution, and Mechanism for the Pyrolysis of Typical Plastic Waste, *ACS Sustainable Chem. Eng.*, 2022, **10**, 91–103.

33 A. Aboulkas, K. El Harfi and A. El Bouadili, Thermal degradation behaviors of polyethylene and polypropylene. Part I: Pyrolysis kinetics and mechanisms, *Energy Convers. Manage.*, 2010, **51**, 1363–1369.

34 C. Abdy, Y. Zhang, J. Wang, Y. Yang, I. Artamendi and B. Allen, Pyrolysis of polyolefin plastic waste and potential applications in asphalt road construction: A technical review, *Resour., Conserv. Recycl.*, 2022, **180**, 106213.

35 D. Choi, S. Jung, S. Lee, K. A. Lin, Y. Park, H. Kim, Y. Tsang and E. Kwon, Leveraging carbon dioxide to control the H_2/CO ratio in catalytic pyrolysis of fishing net waste, *Renewable Sustainable Energy Rev.*, 2021, **138**, 110559.

36 R. Aerts, W. Somers and A. Bogaerts, Carbon Dioxide Splitting in a Dielectric Barrier Discharge Plasma: A Combined Experimental and Computational Study, *ChemSusChem*, 2015, **4**, 702–716.

37 K. Zhang and A. P. Harvey, CO_2 decomposition to CO in the presence of up to 50% O_2 using a non-thermal plasma at atmospheric temperature and pressure, *Chem. Eng. J.*, 2021, **405**, 126625.

38 C. Fromentin, T. Silva, T. Dias, A. Morillo-Candas, O. Biondo, O. Guaitella and V. Guerra, Study of vibrational kinetics of CO_2 and CO in CO_2–O_2 plasmas under non-equilibrium conditions, *Plasma Sources Sci. Technol.*, 2023, **32**, 024001.

39 H. Kang, Y.-N. Kim, H. Song, H. Lee, K.-T. Kim, Y.-H. Song, D. H. Lee and O. L. Li, Feasibility test of a concurrent process for CO_2 reduction and plastic upcycling based on CO_2 plasma jet, *J. CO_2 Util.*, 2021, **52**, 101701.

40 L. M. Martini, G. Dilecce, G. Guella, A. Maranzana, G. Tonachini and P. Tosi, Oxidation of CH_4 by CO_2 in a dielectric barrier discharge, *Chem. Phys. Lett.*, 2014, **593**, 55–60.

41 M. Zeng, Z. Kan, Z. Wang and M. Shen, Carbon isotope effects in the artificial photosynthesis reactions catalyzed

by nanostructured Co/CoO, *Chem. Phys. Lett.*, 2020, **754**, 137731.

42 J. Graciani, K. Mudiyanselage, F. Xu, A. E. Baber, J. Evans, S. D. Senanayake, D. J. Stacchiola, P. Liu, J. Hrbek, J. F. Sanz and J. A. Rodriguez, Highly active copper-ceria and copper-ceria-titania catalysts for methanol synthesis from CO₂, *Science*, 2014, **345**, 546–550.

43 L. Wang, Y. Yi, H. Guo and X. Tu, Atmospheric Pressure and Room Temperature Synthesis of Methanol through Plasma-Catalytic Hydrogenation of CO₂, *ACS Catal.*, 2018, **8**, 90–100.

44 H.-G. Yu, J. T. Muckerman and T. J. Sears, A theoretical study of the potential energy surface for the reaction OH + CO → H + CO₂, *Chem. Phys. Lett.*, 2001, **349**, 547–554.

45 J.-g. Wang, C.-j. Liu, Y.-p. Zhang and B. Eliasson, A DFT study of synthesis of acetic acid from methane and carbon dioxide, *Chem. Phys. Lett.*, 2003, **368**, 313–318.

46 S. Li, J. Sun, Y. Gorbanev, K. van't Veer, B. Loenders, Y. Yi, T. Kenis, Q. Chen and A. Bogaerts, Plasma-Assisted Dry Reforming of CH₄: How Small Amounts of O₂ Addition Can Drastically Enhance the Oxygenate Production—Experiments and Insights from Plasma Chemical Kinetics Modeling, *ACS Sustainable Chem. Eng.*, 2023, **11**, 15373–15384.

47 W. Wang, R. Snoeckx, X. Zhang, M. S. Cha and A. Bogaerts, Modeling Plasma-based CO₂ and CH₄ Conversion in Mixtures with N₂, O₂, and H₂O: The Bigger Plasma Chemistry Picture, *J. Phys. Chem. C*, 2018, **122**, 8704–8723.

48 J. Slaets, M. Aghaei, S. Ceulemans, S. Van Alphen and A. Bogaerts, CO₂ and CH₄ conversion in "real" gas mixtures in a gliding arc plasmatron: how do N₂ and O₂ affect the performance?, *Green Chem.*, 2020, **22**, 1366–1377.

49 T. Thi Bui, L. Pazdur, S. Janssens, V. Vande Velde, P. Billen and S. Tavernier, Production of Long Chain Alcohols from Waste Polyethylene Pyrolysis Oil Using a One-Pot Hydroboration–Oxidation Process, *ACS Sustainable Chem. Eng.*, 2023, **11**, 11729–11736.

50 Z. Xu, N. E. Munyaneza, Q. Zhnag, M. Sun, C. Posada, P. Venturo, N. A. Rorrer, J. Miscall, B. G. Sumpter and G. Liu, Chemical upcycling of polyethylene, polypropylene, and mixtures to high-value surfactants, *Science*, 2023, **381**, 666–671.

51 A. Milbrandt, K. Coney, A. Badgett and G. T. Beckham, Quantification and evaluation of plastic waste in the United States, *Resour., Conserv. Recycl.*, 2022, **182**, 106363.

52 U. R. Gracida-Alvarez, O. Winjobi, J. C. Sacramento-Rivero and D. R. Shonnard, System Analyses of High-Value Chemicals and Fuels from a Waste High-Density Polyethylene Refinery. Part 1: Conceptual Design and Techno-Economic Assessment, *ACS Sustainable Chem. Eng.*, 2019, **7**, 18254–18266.

53 O. Olafasakin, J. Ma, S. L. Bradshaw, H. A. Aguirre-Villegas, C. Benson, G. W. Huber, V. M. Zavala and M. Mba-Wright, Techno-Economic and life cycle assessment of standalone

54 Single-Stream material recovery facilities in the United States, *Waste Manage.*, 2023, **166**, 368–376.

54 Environmental Research and Educational Foundation, Analysis of MSW Landfill Tipping Fees, available at: https://www.erefdn.org, accessed March 23, 2024.

55 A. Badgett, G. Cooney, J. Hoffmann and A. Milbrandt, CO₂ Emissions from Stationary Sources, *2023 Billion-Ton Report*, M. H. Langholtz (Lead), Oak Ridge National Laboratory, 2024, ch. 7.3.

56 T. N. Do, C. You and J. Kim, A CO₂ utilization framework for liquid fuels and chemical production: techno-economic and environmental analysis, *Energy Environ. Sci.*, 2022, **15**, 169–184.

57 J. Kim, T. A. Johnson, J. E. Miller, E. B. Stechel and C. T. Maravelias, Fuel production from CO₂ using solar-thermal energy: system level analysis, *Energy Environ. Sci.*, 2022, **15**, 169–184.

58 ChemAnalyst, Paraffin Wax Price Trend and Forecast, available at: https://www.chemanalyst.com/Pricing-data/paraffin-wax-1205, accessed November 10, 2023.

59 ChemAnalyst, Linear Alpha Olefin Price Trend and Forecast, available at: https://www.chemanalyst.com/Pricing-data/linear-alpha-olefin-1103, accessed November 10, 2023.

60 ChemAnalyst, Paraformaldehyde Price Trend and Forecast, available at: https://www.chemanalyst.com/Pricing-data/paraformaldehyde-pfa-1195, accessed November 10, 2023.

61 J. Hambalko, P. Gajdoš, J. M. Nicaud, *et al.*, Production of Long Chain Fatty Alcohols Found in Bumblebee Pheromones by *Yarrowia lipolytica*, *Front. Bioeng. Biotechnol.*, 2020, **8**, 593419.

62 R. Wang, Y. Luo, H. Jia, J. R. Ferrell and H. Ben, Development of quantitative ¹³C NMR characterization and simulation of C, H, and O content for pyrolysis oils based on ¹³C NMR analysis, *RSC Adv.*, 2020, **10**, 25918–25928.

63 R. Partington, J. Clarkson, J. Paterson, K. Sullivan and J. Wilson, Quantitative carbon distribution analysis of hydrocarbons, alcohols, and carboxylic acids in a Fischer-Tropsch product from a Co/TiO₂ catalyst during gas phase pilot plant operation, *J. Anal. Sci. Technol.*, 2020, **11**, 42.

64 R. J. Speight, ¹H and ¹³C solution- and solid-state NMR investigation into wax products from the Fischer–Tropsch process, *Solid State Nucl. Magn. Reson.*, 2011, **39**, 58–64.

65 Y. Cortes-Peña, D. Kumar, V. Singh and J. S. Guest, BioSTEAM: A Fast and Flexible Platform for the Design, Simulation, and Techno-Economic Analysis of Biorefineries under Uncertainty, *ACS Sustainable Chem. Eng.*, 2020, **8**, 3302–3310.

66 D. Humbird, R. Davis and L. Tao, Process Design and Economics for Biochemical Conversion of Lignocellulosic Biomass to Ethanol: Dilute-Acid Pretreatment and Enzymatic Hydrolysis of Corn Stover, NREL/TP-5100-47764, 1013269, 2011.

67 openLCA Modeling Suite, GreenDelta GmbH, Berlin, Germany, 2023, available at: https://www.openlca.org/openlca/, accessed November 30, 2023.